AIMS Energy, 14(6): 1299–1343.
DOI: 10.3934/energy.2026051
Received: 22 July 2026
Revised: 24 September 2026
Accepted: 15 October 2026
Published: 02 November 2026

https://www.aimspress.com/journal/energy

Review

A comprehensive review of mixture formation and combustion mechanisms in port-fuel-injected hydrogen spark-ignition engines

Pham Van Trong, Nguyen Duy Vinh* and Hoang Dinh Long

Faculty of Vehicle and Energy Engineering, Phenikaa School of Engineering, Phenikaa University, Vietnam

* **Correspondence:** Email: Vinh.nguyenduy@phenikaa uni.edu.vn; Tel: +84-985814118.

Abstract: Hydrogen-fueled spark-ignition engines represent a compelling technical pathway toward decarbonized transportation, combining zero-carbon tailpipe emissions with high thermodynamic efficiency and direct compatibility with existing manufacturing architectures. Among fuel-delivery methods, port fuel injection remains particularly useful because it is cost-effective, has low system complexity, and is easy to retrofit onto conventional gasoline platforms. Nevertheless, hydrogen's distinct physicochemical characteristics, namely its low minimum ignition energy, broad flammability range, high laminar burning velocity, low volumetric density, and rapid molecular diffusivity, fundamentally alter mixture homogenization, flame development, thermal efficiency, and emission profiles compared to those of conventional hydrocarbon fuels. This paper provides a critical, systematic review of the mechanisms governing mixture preparation and combustion behavior in PFI hydrogen SI engines. We thoroughly scrutinize key phenomena—including in-port mixing dynamics, in-cylinder flow fields, flame propagation kinetics, heat release rates, cyclic stability, abnormal combustion vulnerabilities (backfire, surface pre-ignition, and knock), and thermal NOx formation pathways. The review also comprehensively evaluates the operational impacts of primary control parameters, such as excess air ratio, spark phasing, compression ratio, injection strategy, engine load, engine speed, exhaust gas recirculation, and intake boosting. By synthesizing multidimensional computational fluid dynamics models, one-dimensional thermodynamic simulations, and bench-scale experimental data, this review identifies technological milestones and prevailing bottlenecks. Finally, unresolved technical barriers are outlined alongside prospective research trajectories, including optimized injection dynamics, intelligent closed-loop combustion control, dual-fuel synergies, and holistic system optimization, to accelerate the realization of high-efficiency, ultra-low-emission hydrogen powertrains for next-generation mobility.

Keywords: hydrogen engine; port fuel injection; spark ignition; mixture formation; hydrogen combustion; flame propagation; NOx emissions

1. Introduction

The escalating demand for sustainable transportation pathways, coupled with stringent international mandates to mitigate greenhouse gas emissions, has intensified global research into alternative energy carriers for internal combustion engines. Rapid development of the social economy accelerates fossil fuel consumption, carbon dioxide emissions, and hazardous pollutant emissions, including nitrogen oxides and particulate matter [1]. The provided sources offer a comprehensive overview of the background, advantages, and technical frameworks of hydrogen-fueled internal combustion engines, with a particular focus on SI engines with PFI. The transition toward hydrogen energy is primarily driven by the urgent global need to mitigate climate change and meet the carbon neutrality targets set by international agreements such as the Paris Agreement and the Glasgow Agreement. The transportation sector accounts for a significant share of global greenhouse gas emissions, and hydrogen engines provide a path to zero tailpipe CO_2 emissions [2]. The depletion of fossil fuel reserves and rising prices drive interest in renewable and abundant energy carriers like hydrogen, which can be produced from diverse sources including water electrolysis. Also, unlike electric vehicles, hydrogen internal combustion engines leverage over a century of established manufacturing facilities and workforce know-how, allowing for a faster and more affordable transition than fuel cells [3].

Hydrogen engines—encompassing both direct-injection and port-injection types—offer distinct advantages [4]. They outperform other zero-emission technologies across multiple key performance metrics, including driving range, refueling time, thermal efficiency, durability, and environmental compatibility [5,6]. As a prominent carbon-free energy carrier, hydrogen combustion fundamentally eliminates tailpipe emissions of carbon dioxide, carbon monoxide, unburned hydrocarbons, and particulate matter, thereby paving a direct pathway toward net-zero carbon transportation [7,8]. Furthermore, hydrogen boasts an exceptionally high gravimetric energy density, with a lower heating value of approximately 120 MJ/kg, which is roughly 2.7–3 times greater than that of conventional gasoline or diesel fuels [5,6]. This superior energy density holds substantial potential for enhancing overall engine efficiency while lowering specific fuel consumption. The abbreviations and symbols used throughout this review are summarized in Table 1.

Table 1. Abbreviations and symbols used in the study of hydrogen-fueled ICEs.

Abbreviations and symbols	Definition	Abbreviations and symbols	Definition
A/F	Air-fuel ratio	H_2O	Water
ATDC	After top dead center	HC	Unburned hydrocarbons
BDC	Bottom dead center	HRR	Heat release rate
BEV	Battery electric vehicle	IEGR	Internal exhaust gas recirculation
BMEP	Brake mean effective pressure	IMEP	Indicated mean effective pressure

Continued on next page

Abbreviations and symbols	Definition	Abbreviations and symbols	Definition
BTE	Brake thermal efficiency	ITE	Indicated thermal efficiency
BTDC	Before top dead center	IVC/IVO	Intake valve close/intake valve open
CA	Crank angle	LBV	Laminar burning velocity
CA50	Crank angle at 50% mass fraction burned	LDI	Late direct injection
CCV	Cycle-to-cycle variation	LES	Large eddy simulation
CFD	Computational fluid dynamics	LHV	Lower heating value
CO	Carbon monoxide	LPG	Liquefied petroleum gas
CO_2	Carbon dioxide	MBT	Maximum brake torque
COVIMEP	Coefficient of variation of indicated mean effective pressure	MFB	Mass fraction burned
CR	Compression ratio	NOx	Nitrogen oxide
DISI	Direct injection spark ignition	PM	Particulate matter
EGR	Exhaust gas recirculation	PEM/PEMFC	Proton exchange membrane fuel cell
EGT	Exhaust gas temperature	H2ICE/H_2ICE	Hydrogen internal combustion engine
EOI	End of injection	PEMC	Pre-ignition in the early/mid-compression stroke
EVO	Exhaust valve open	PLC	Pre-ignition in the late-compression stroke
FCEV	Fuel cell electric vehicle	PFI/H_2PFI	Port fuel injection/hydrogen port fuel injection
GHG	Greenhouse gas	PLIF	Planar laser-induced fluorescence
ppm	Parts per million	RON/MON	Research octane number/motor octane number
PRR	Pressure rise rate	TJI	Turbulent jet ignition
RANS	Reynolds-averaged Navier-Stokes	WHR	Water-to-hydrogen ratio
RF	Random forest	WI	Water injection
SI	Spark ignition	1D	One-dimensional
SOI	Start of injection	λ	Excess air ratio
PRR	Pressure rise rate		

In the context of transportation decarbonization, selecting among BEVs, FCEVs, and H2ICEs involves multidimensional trade-offs among energy efficiency, economic feasibility, and operational robustness [3]. BEVs demonstrate superior tank-to-wheel energy efficiency due to direct electrochemical-to-mechanical energy conversion. However, their widespread daily utility remains moderately constrained by restricted driving ranges, prolonged charging durations, and substantial infrastructure and battery-related capital expenditures. Conversely, hydrogen-based powertrains effectively overcome these operational hurdles by providing rapid refueling times comparable to conventional liquid-fueled vehicles and extended driving ranges, making them particularly suitable for long-haul and heavy-duty applications [3]. Within the hydrogen domain, distinctive technical compromises emerge between electrochemical and thermodynamic pathways. FCEVs deliver outstanding climate protection with zero harmful carbon tailpipe emissions, yet they are burdened by exorbitant manufacturing costs, hydrogen fueling infrastructure expenses, and premature membrane-electrode assembly degradation under dynamic operating cycles. In contrast, H2ICEs capitalize on mature internal combustion engine architectures and established production lines, which markedly reduce capital expenditure while providing superior mechanical durability and high tolerance to fuel impurities. Although H2ICE thermal efficiency is naturally capped by thermodynamic combustion limits compared to the peak efficiency of BEVs, both H2ICEs and FCEVs offer exceptional greenhouse gas reduction potential. Consequently, H2ICE technology stands out as a practical, durable, and cost-effective decarbonization pathway for modern automotive propulsion systems.

In addition to its favorable energy content, hydrogen possesses unique physicochemical properties that facilitate high-efficiency internal combustion. Its exceptionally wide flammability limits in air—spanning from approximately 4% to 75% by volume—enable stable engine operation under ultra-lean conditions, which simultaneously improves thermal efficiency and suppresses thermal NO_x formation [1,8]. Moreover, hydrogen exhibits a laminar flame speed roughly 5.5–10 times higher than that of gasoline [7]. This characteristic promotes rapid heat release rates that closely approximate the ideal constant-volume combustion cycle of the Otto cycle. Coupled with an extremely low ignition energy requirement of approximately 0.02 mJ, hydrogen ensures reliable ignition during cold starts and sustains stable combustion across ultra-lean mixtures [9,10]. Hydrogen's high mass diffusion coefficient—approximately 12 times that of gasoline—significantly accelerates fuel-air mixing kinetics, facilitating the creation of highly homogeneous combustible charges within the intake system [11]. This high diffusivity also enhances operational safety by allowing leaked hydrogen to dissipate rapidly into the atmosphere, thereby mitigating the risks of localized accumulation and hazardous ignition [9,10]. Collectively, these unique thermophysical and combustion properties establish hydrogen as an exceptionally promising fuel for achieving high-efficiency, near-zero-emission, and sustainable internal combustion engine technologies.

Among the various hydrogen fueling strategies for SI engines, PFI has emerged as one of the most practical and extensively investigated approaches for near-term implementation. A primary advantage of PFI systems lies in their simplicity and cost-effectiveness; compared with direct injection technologies, they require relatively minor modifications to conventional gasoline engines and operate at low fuel delivery pressures typically below 0.5 MPa, thereby reducing system complexity and capital costs [11–13]. Furthermore, PFI technology promotes superior fuel-air mixture homogenization by allowing sufficient mixing time within the intake manifold or port prior to combustion chamber entry. This enhanced mixture uniformity yields improved combustion stability and reduced cycle-to-cycle variations [14–16]. This is particularly advantageous for lean-burn operation.

Capitalizing on the maturity of existing SI engine manufacturing infrastructures and supply chains, PFI hydrogen engines serve as a pragmatic bridge technology that accelerates commercial adoption while contributing to near-term greenhouse gas mitigation [3].

Building upon these advantages, current research efforts are directed toward addressing the remaining technical challenges that hinder large-scale commercialization. Despite significant progress in H2ICE research, primary objectives focus on systematically understanding and suppressing abnormal combustion phenomena—such as backfire, pre-ignition, and knock—which are exacerbated by hydrogen's low ignition energy, high flame speed, and wide flammability limits [10,12,17]. Mitigating these undesirable events is critical for ensuring operational reliability and safety. Another major research focus involves controlling NOx emissions, the principal pollutant generated under stoichiometric and high-load thermal conditions, through advanced strategies such as exhaust gas recirculation, water injection, and ultra-lean combustion [2,3]. Moreover, considerable attention has been directed toward optimizing PFI operating parameters (e.g., injection timing, duration, supply pressure, and nozzle geometry) to maximize volumetric efficiency and combustion stability. By synthesizing these developments, ongoing studies aim to support the realization of efficient, reliable, and sustainable hydrogen-powered transportation systems.

To deliver a comprehensive and scientifically rigorous assessment of this evolving field, this review employs a systematic literature analysis integrated with numerical simulations and experimental data. Large-scale literature syntheses, encompassing over 150 peer-reviewed articles, serve to outline global development trends and technological milestones [1]. In addition, comparative analyses evaluate PFI versus DI systems, as well as hydrogen relative to alternative low-carbon fuels such as methane and ammonia. Numerically, 1D and CFD simulation frameworks—utilizing platforms such as AVL BOOST and ANSYS Forte—are widely adopted to examine mixture formation, heat transfer, and pollutant kinetics. The integration of detailed chemical kinetic mechanisms and numerical models, rigorously validated against high-precision engine test bench data, establishes a robust methodological framework for accelerating H2ICE design, optimization, and future technological advancement.

2. Hydrogen fuel characteristics and fundamental properties

2.1. Physicochemical properties of hydrogen

Hydrogen possesses unique physicochemical properties that distinguish it from conventional hydrocarbon fuels, offering significant potential as a clean alternative energy source for internal combustion engines while introducing specific technical challenges. As summarized in Table 2, hydrogen exhibits an LHV of approximately 120 MJ/kg, which is the highest among chemical fuels and roughly 2.5–3 times greater than that of gasoline (44.4 MJ/kg) and methane (50 MJ/kg). This exceptional gravimetric energy density makes hydrogen an attractive candidate for high-efficiency energy conversion systems with zero carbon emissions at the point of use. However, despite its high energy content per unit mass, hydrogen features an extremely low density under standard conditions, resulting in a very low volumetric energy density [10,18]. Consequently, fuel storage, transportation, and onboard packaging remain critical barriers to widespread commercial utilization.

From a mixture formation perspective, hydrogen requires a stoichiometric A/F mass ratio of approximately 34.3:1, which is considerably higher than that of conventional fuels [10,19]. Under

stoichiometric conditions, hydrogen occupies roughly 29.6% of the combustion chamber volume (Table 2), thereby displacing a significant amount of fresh inducted air [19]. This displacement effect reduces volumetric efficiency and can constrain the maximum power output of port fuel-injected hydrogen engines, particularly under high-load operations. Nevertheless, hydrogen possesses a remarkably high mass diffusion coefficient in ambient air (0.61 cm^2/s, Table 2), enabling rapid fuel-air mixing and facilitating the formation of highly homogeneous combustible charges. Furthermore, this high diffusivity enhances operational safety by promoting rapid dissipation in the event of a leak, thereby minimizing localized fuel accumulation.

Table 2. Comparison of physicochemical properties between hydrogen and conventional fuels [3].

Property	Hydrogen	Methane	Gasoline	Diesel
Carbon content (mass %)	0	75	84	86
LHV (MJ/kg)	119.9	45.8	43.9	42.5
Density (at bar and 273 K; kg/m^3)	0.089	0.7	730–780	830
Volumetric energy content (at 1 bar and 273 K, MJ/m^3)	10.7	33	33×10^3	35×10^3
Stoichiometric air-fuel ratio A/F	34.4	17.2	14.7	14.5
Minimum ignition energy (at 1 bar and 298 K and stoichiometry, mJ)	0.02	0.29	0.24	0.24
Flammability limits in air (at 1 bar and 298 K and stoichiometry, vol%)	4.0–76.0	5.3–15.0	1.0–7.6	0.6–5.5
Laminar flame speed in air (at 1 bar and 298 K, m/s)	1.85	0.38	0.37–0.40	0.37–0.43
Quenching distance (at 1 bar and 298 K and stoichiometry, mm)	0.64	2.1	2	–
Diffusion coefficient in air (at 1 bar and 273 K, m^2/s)	8.5×10^{-6}	1.9×10^{-6}	–	–
Auto-ignition temperature (K)	858	813	623	523
Octane number (RON)	130+	120+	91–98	–
Cetane number			13–17	40–55

Hydrogen's combustion characteristics further differentiate it from traditional fuels. As illustrated in Figure 1, hydrogen requires an exceptionally low minimum ignition energy (approximately 0.02 mJ, Table 2), which is nearly an order of magnitude lower than that of conventional hydrocarbons such as methane, ethane, propane, and butane. In addition, as shown in Figure 2, hydrogen exhibits an exceptionally wide flammability range, sustaining stable combustion in air across concentrations from roughly 4% to 75% by volume. This property enables stable engine operation under ultra-lean conditions, enhancing thermal efficiency while suppressing thermal NO_x formation via reduced combustion temperatures [20]. Although this broad flammability range facilitates reliable ignition and extends lean-burn capabilities, it concurrently heightens sensitivity to unintended ignition sources within the combustion chamber, rendering hydrogen engines considerably more susceptible to abnormal combustion phenomena, such as pre-ignition and backfire [10,12,21].

Another critical feature of hydrogen combustion is its high laminar burning velocity, ranging from approximately 2.65 to 3.25 m/s under standard conditions—nearly seven times higher than that of gasoline (0.40 m/s, Table 2) [10,18,22]. This rapid flame propagation shortens combustion duration, allowing the thermodynamic cycle to closely approach the ideal constant-volume Otto cycle, thereby improving thermal efficiency and combustion stability. However, hydrogen also exhibits a very small quenching distance (approximately 0.60–0.64 mm, Table 2), which is substantially lower than that of gasoline (2.00 mm) [10,18]. Consequently, hydrogen flames can propagate into narrow crevices, such as piston ring lands and confined combustion chamber geometries, making flame extinction more

difficult and compounding the risks of backfire and pre-ignition [18,19,23]. Conversely, hydrogen demonstrates robust resistance to knock, underpinned by a high auto-ignition temperature (858 K) and a high research octane number (RON > 130) [10,18,19]. These traits allow spark-ignition hydrogen engines to operate at significantly higher compression ratios than conventional gasoline engines without inducing auto-ignition, offering further potential for thermal efficiency enhancements.

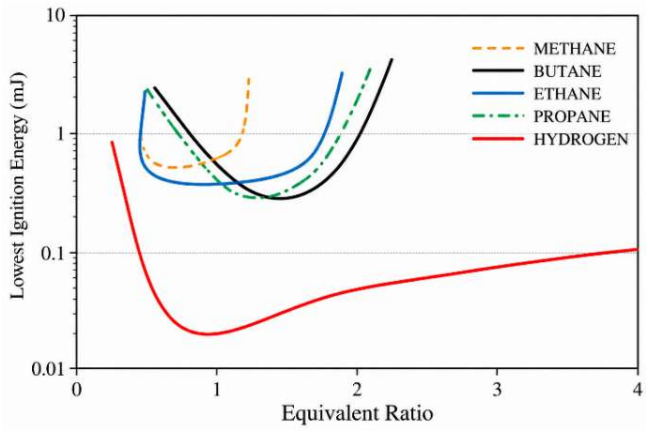


Figure 1. Minimum ignition energy versus equivalence ratio for different gas-air mixtures.

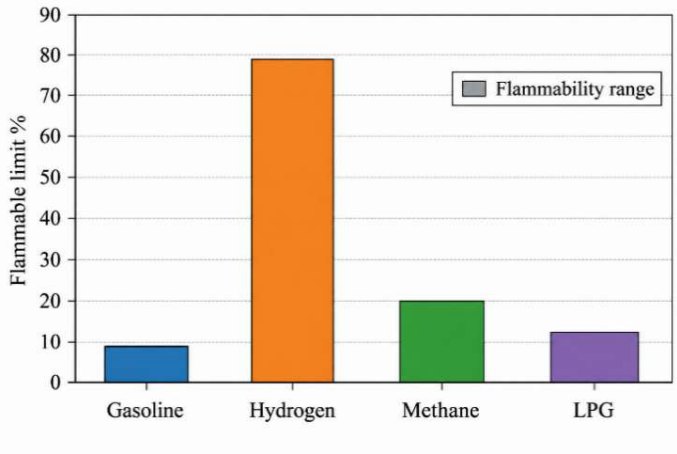


Figure 2. Flammability limit (%) for different fuels.

From an environmental perspective, hydrogen offers a substantial advantage due to its carbon-free chemical structure. Theoretical hydrogen combustion produces no carbon-containing emissions, thereby virtually eliminating tailpipe outputs of CO_2, CO, HC, and PM [12,22]. Trace amounts of these species observed in practical engine exhaust are typically attributed to lubricating oil consumption and oxidation rather than the fuel itself [10,19,22]. Nevertheless, despite being carbon-free, hydrogen combustion can still generate significant NOx owing to its relatively high adiabatic flame temperature, which typically spans from 2379 K to 2480 K under stoichiometric conditions [10,18,24]. These elevated temperatures promote thermal NO_x formation via the extended Zeldovich mechanism, particularly during stoichiometric or high-load operations, representing one of the foremost challenges in the development of hydrogen internal combustion engines.

2.2. Advantages and technical implications in SI engines

Hydrogen is widely recognized as one of the most promising alternative fuels for SI internal combustion engines, offering substantial advantages in emissions reduction, thermal efficiency, combustion performance, and practical implementation [12,21,22]. From an environmental standpoint, hydrogen combustion theoretically eliminates direct carbon-containing emissions—such as carbon dioxide, carbon monoxide, unburned hydrocarbons, and particulate matter—while supporting a near-zero-carbon well-to-wheel pathway when produced renewably [10,22,25]. Furthermore, hydrogen significantly enhances thermal efficiency through unthrottled quality governing, high laminar flame speeds, and high autoignition temperatures (approximately 858 K), coupled with a high octane rating exceeding 130, permitting elevated compression ratios (12–15 or higher) without knock. From a combustion perspective, its exceptionally wide flammability range (4%–75% by volume in air), low ignition energy, and high diffusion coefficient facilitate reliable cold-start performance, rapid mixture preparation, and enhanced combustion completeness in crevice regions [3,18,22]. Industrially, existing engine platforms can be adapted through moderate modifications to serve as a practical, cost-effective transitional solution [17,26] with high fuel impurity tolerance and enhanced safety characteristics due to rapid atmospheric dispersion [17,27,28].

Despite its significant potential as a carbon-free energy carrier, the widespread commercialization of hydrogen internal combustion engines remains constrained by interrelated challenges spanning storage, engine operation, material compatibility, and fueling infrastructure. A primary physical limitation arises from hydrogen's extremely low volumetric energy density, necessitating high-pressure compression (350–700 bar) or cryogenic liquefaction (−2530 °C) in costly, heavy storage vessels, compounded by high leakage and permeation rates. Operationally, favorable combustion traits concurrently exacerbate abnormal combustion phenomena, such as intake backfire, pre-ignition, and excessive pressure rise rates due to low ignition energy and rapid flame propagation [22,23]. Moreover, gaseous hydrogen displacement reduces volumetric efficiency and power output under stoichiometric conditions, while high adiabatic flame temperatures promote thermal NOx formation, which lean-burn strategies can only partially mitigate at the expense of engine power [3,11,24]. Material durability is further challenged by hydrogen embrittlement, low lubricity accelerating mechanical wear, and potential crankcase gas accumulation [3,29–31].

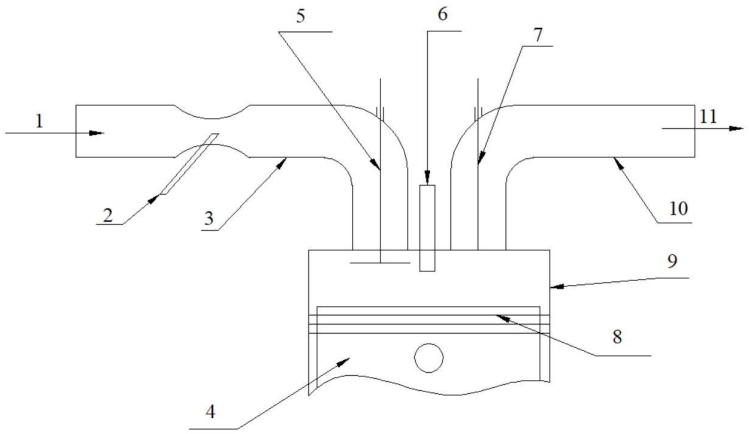
Finally, economic and infrastructure hurdles—including the high cost of green hydrogen production compared to steam methane reforming, massive capital requirements for refueling networks, and stringent safety management due to odorless leaks—underscore the necessity for harmonized international standards and continued technological development [1,3,17].

3. Mixture formation mechanisms in port-fuel-injected hydrogen engines

3.1. PFI architecture and operating fundamentals

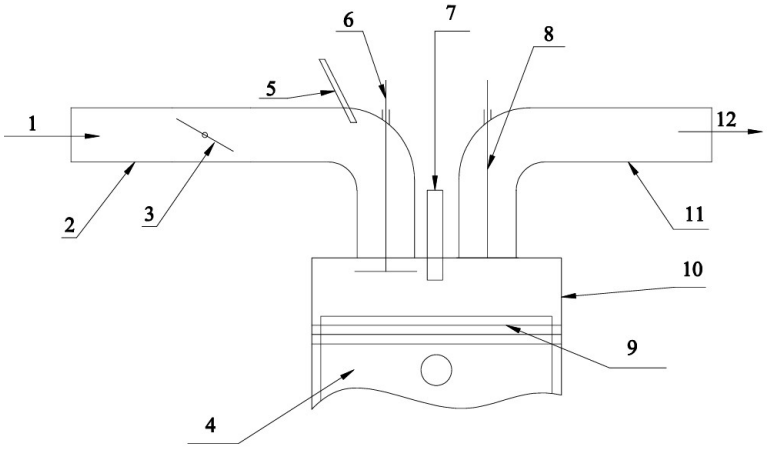
PFI remains the predominant and most technologically mature strategy for hydrogen internal combustion engines, primarily owing to its seamless compatibility with conventional architectures and the minimal hardware retrofitting required [22]. Compared to more intricate injection methods, PFI offers a cost-effective pathway for the near-term commercialization of hydrogen spark-ignition engines. Unlike central carburetion configurations (Figures 3 and 4), hydrogen PFI introduces fuel into the

intake manifold or directly targeted at each cylinder's intake port, upstream of the intake valve. Injection timing is typically phased after the start of the intake stroke using electronically actuated solenoid injectors. This upstream delivery enables external premixing with the incoming air charge before cylinder entry, thereby establishing a well-defined premixed combustion regime [3]. A definitive operational benefit of the PFI configuration is the rapid formation of a highly homogeneous in-cylinder mixture before spark ignition. This charge homogeneity significantly enhances combustion stability, minimizes cycle-to-cycle variations, and ensures robust operation across wide load ranges [32]. Crucially, the uniformly dispersed charge facilitates stable ultra-lean burn strategies, driving higher thermal efficiencies while effectively attenuating peak in-cylinder temperatures and, consequently, suppressing NOx emissions [3,24].



1–Air, 2–Hydrogen fuel, 3–Intake pipe, 4–Piston, 5–Intake vale, 6–Spark plug, 7–Exhaust vale, 8–Piton ring, 9–Cylinder, 10–Exhaust pipe, 11–Exhaust gas.

Figure 3. Fuel carburetion method [19].



1–Air, 2–Intake pipe, 3– Throle, 4–Piston, 5–Injection hydrogen fuel, 6–Intake vale, 7–Spark plug, 8–Exhaust vale, 9–Piton ring, 10–Cylinder, 11–Exhaust pipe, 12–Exhaust gas.

Figure 4. Inlet manifold and port injection [19].

Another prominent operational advantage of PFI lies in its moderate injection pressure requirements [31]. In contrast to direct-injection configurations operating against high in-cylinder backpressures, PFI systems function within a modest pressure window of 0.2–1.0 MPa (2–10 bar) [11,33]. This benign operating regime considerably simplifies the fuel rail architecture, lowers capital costs, and circumvents the stringent durability, sealing, and material degradation challenges typical of high-pressure fueling loops. Critical injector failure modes—notably, impact wear at the nozzle tip, frictional erosion along needle guides, coating embrittlement, and dielectric degradation in piezoelectric actuators—are significantly exacerbated under extreme pressure gradients, which compromise sealing integrity and metering accuracy over extended operating cycles [6]. Notwithstanding these benefits, hydrogen PFI is inherently constrained by volumetric displacement penalties within the intake tract [11]. Introducing gaseous hydrogen upstream displaces incoming air, occupying roughly 30% of the inducted mixture volume under stoichiometric conditions. This pronounced charge displacement diminishes cylinder volumetric efficiency and restricts total oxygen mass induction [28,34]. Consequently, PFI hydrogen engines typically suffer a 15%–30% derating in peak power density relative to baseline gasoline engines of equivalent displacement [3,11].

3.2. Hydrogen-mixing kinetics in the intake runner

The hydrogen-air mixing process plays a pivotal role in determining combustion efficiency, operational stability, and emission characteristics in hydrogen-fueled spark-ignition engines. In PFI hydrogen engines, mixture preparation occurs entirely within the intake port and manifold prior to cylinder induction, resulting in unique mixing dynamics governed by hydrogen's physical properties and the injection strategy employed. Owing to its exceptionally high molecular diffusivity, hydrogen disperses rapidly within the intake airflow, promoting the formation of a highly homogeneous combustible mixture [1]. This diffusion coefficient is substantially greater than that of conventional hydrocarbon fuels, enabling more effective fuel-air mixing during the intake process [3].

A key advantage of the PFI configuration is the relatively long residence time available between fuel injection and intake valve closure. During this period, turbulent mixing and molecular diffusion act synergistically to reduce local concentration gradients, thereby enhancing mixture homogeneity before the charge enters the combustion chamber. Consequently, the quality of the premixed charge is strongly influenced by the start-of-injection timing, which governs the temporal and spatial evolution of hydrogen concentration within the intake system. Early injection strategies provide the longest mixing duration and therefore facilitate the most uniform hydrogen distribution throughout the intake flow [22]. Under such conditions, hydrogen has sufficient time to interact with the incoming air stream, resulting in a nearly homogeneous mixture at the onset of combustion. In contrast, intermediate SOI timings, typically corresponding to approximately 20%–30% of the intake valve lift, can generate a stratified flow structure characterized by alternating layers of air and hydrogen-enriched mixtures [22]. However, delaying the injection event reduces the available mixing time and consequently increases concentration inhomogeneity. Late injection may lead to localized hydrogen accumulation near the intake valve region, creating fuel-rich pockets that significantly increase the risk of backfire and abnormal combustion phenomena within the intake manifold [22].

3.3. In-cylinder flow characteristics and flow field

The transient in-cylinder flow dynamics in hydrogen internal combustion engines are primarily dictated by the aerodynamic coupling between high-momentum gaseous fuel jets and bulk charge motion, specifically tumble and swirl [35–37]. In PFI architectures, the extended residence time within the intake tract enables effective charge premixing before intake valve closure [35]. Distinct from conventional liquid diesel sprays, underexpanded hydrogen jets generate coherent recirculating flow structures, predominantly characterized as head vortices or a "vortex-ball" topology [38]. These vortical structures intensify turbulent shear layers, promote lateral jet expansion, and drive intense air entrainment into the jet core, yielding entrainment rates up to threefold higher than those observed in standard liquid sprays [38].

The spatial distribution and turbulence kinetic energy within the cylinder are further modulated by injector nozzle geometry and combustion chamber boundaries. Multi-hole nozzle configurations demonstrate superior mixture homogenization compared to hollow-cone geometries; the mutual interaction and shear among adjacent discrete macro-jets break down into higher-frequency turbulent eddies. This cascade accelerates turbulent dissipation and yields a more uniformly dispersed charge across the cylinder volume [37]. Overall, the mixture preparation is governed by a tightly coupled set of operating and design parameters, predominantly SOI, injection pressure, nozzle topology, and background in-cylinder aerodynamics [22].

As depicted in Figure 5, the in-cylinder hydrogen trapped mass is acutely sensitive to injection phasing and orientation. Peak trapped mass is achieved within an injection window of 380° to 420° CA. Deviations from this optimal window incur fuel induction penalties through two distinct mechanisms: premature injection phases lead to charge backflow into the runner during pressure fluctuations, whereas excessively delayed injection results in residual fuel entrapment upstream of the closed intake valve, failing to be inducted within the active cycle.

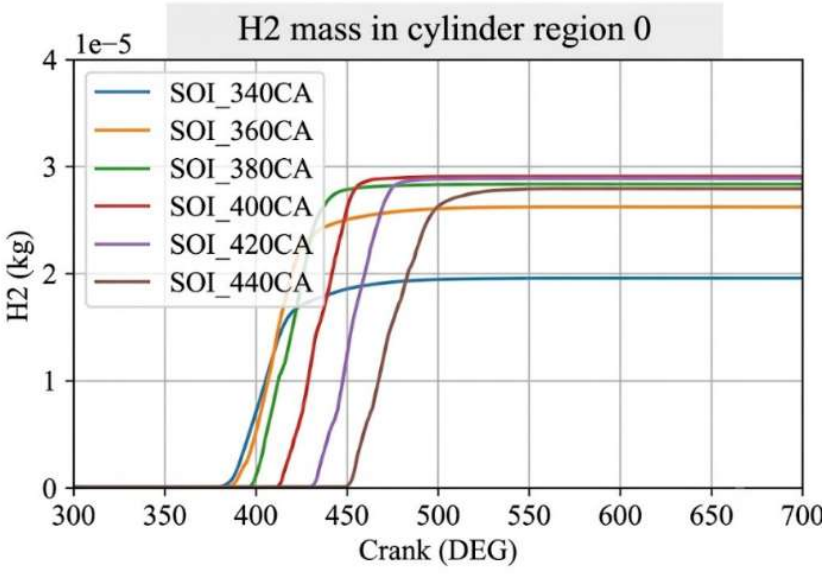


Figure 5. Hydrogen mass in key computational regions as a function of start of injection (SOI) timing [22].

Elevating injection pressure enhances jet momentum and turbulence intensity via higher nozzle exit velocities, thereby expediting turbulent mass transfer and charge homogenization [39]. Furthermore, as illustrated in Figure 6, nozzle topology—governed by nozzle architecture, orifice count, and hole diameter—in conjunction with injector spatial location and spray trajectory, fundamentally shapes the spatial distribution of the fuel charge throughout the cylinder volume [37].

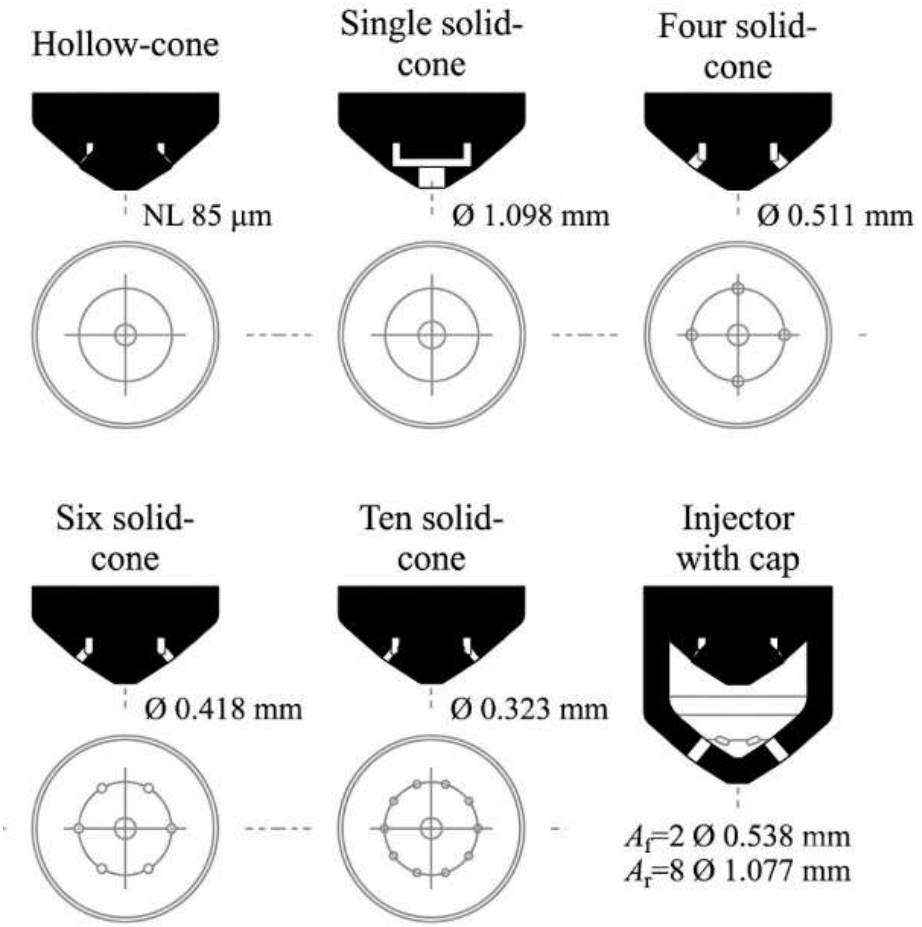


Figure 6. Injector geometry and hole size comparison [37].

As illustrated in Figures 7 and 8, in-cylinder tumble and swirl aerodynamic structures intensify turbulent shear, thereby accelerating spatial fuel dispersion and charge homogenization [37]. While gaseous injection promotes rapid mixture formation with the inducted air, it inherently triggers an air-displacement penalty that constrains cylinder volumetric efficiency. Furthermore, injection duration serves as a critical governing parameter: shorter durations facilitate rapid charge premixing and yield superior mixture uniformity, whereas excessively prolonged injection profiles compromise charge homogeneity and risk unburned fuel entrapment as injection events encroach upon intake valve closure.

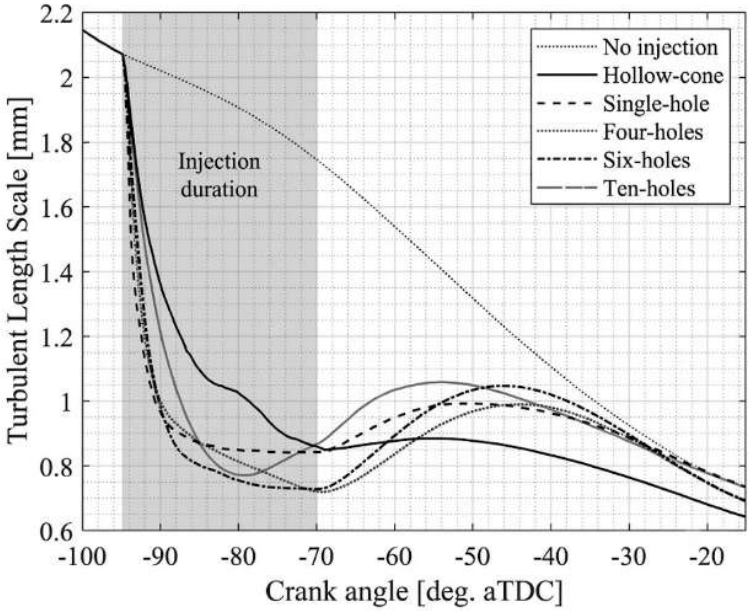


Figure 7. In-chamber turbulent length scale for different injector designs [37].

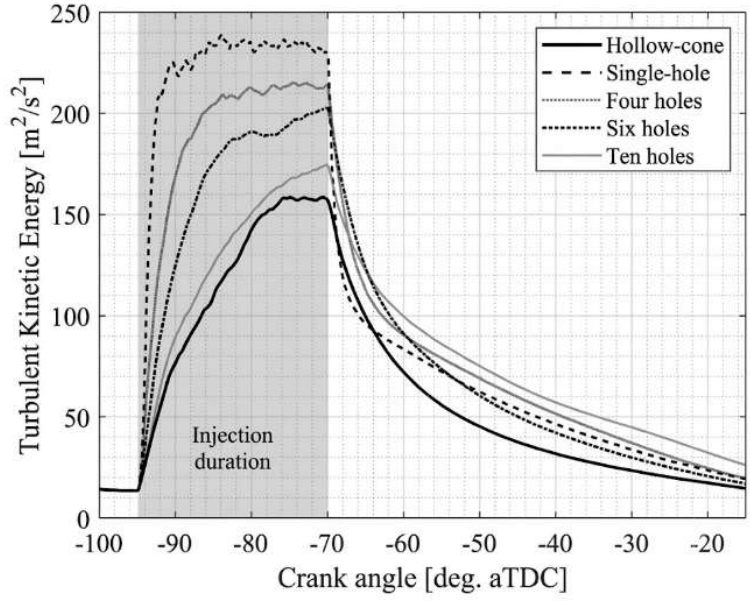


Figure 8. In-chamber turbulent kinetic energy for different injector designs [37].

3.4. Challenges in mixture preparation

For PFI hydrogen engines, mixture preparation is primarily challenged by hydrogen's low density and high reactivity. The gaseous fuel displaces a significant portion of the air intake, reducing volumetric efficiency and limiting engine power output. Furthermore, hydrogen's extremely low ignition energy and wide flammability range make PFI systems highly susceptible to backfire, as combustible mixtures can be ignited by hot spots or residual gases in the intake manifold.

As demonstrated in Figure 9, injection phasing critically governs mixture preparation and backfire propensity in hydrogen PFI engines. An excessively advanced SOI prolongs the residence time of gaseous fuel within the intake runner, yielding localized residual accumulation that sharply elevates backfire risks [12]. Conversely, an overly delayed EOI leaves a fraction of uninducted fuel stranded upstream of the closing valve, promoting backfire events in subsequent operating cycles. Consequently, the optimal injection window coincides with the period of peak intake valve lift—typically within an SOI range of 390º to 430° CA—which balances adequate premixing with minimal intake manifold charge entrapment [12]. While rapid premixing benefits charge homogeneity, the accelerated rate of mixture dispersion introduces operational challenges in precisely modulating spatial stratification and combustion phasing [3,22] Furthermore, dry operating interfaces and stringent sealing requirements aggravate frictional wear, inter-component leakage, and hardware durability limits within the injector assembly. Lean-burn strategies are widely implemented to mitigate peak temperatures and suppress thermal NO_x formation; however, pushing beyond the stable lean threshold induces severe combustion instability, elevated cyclic variability, and occasional misfire [39].

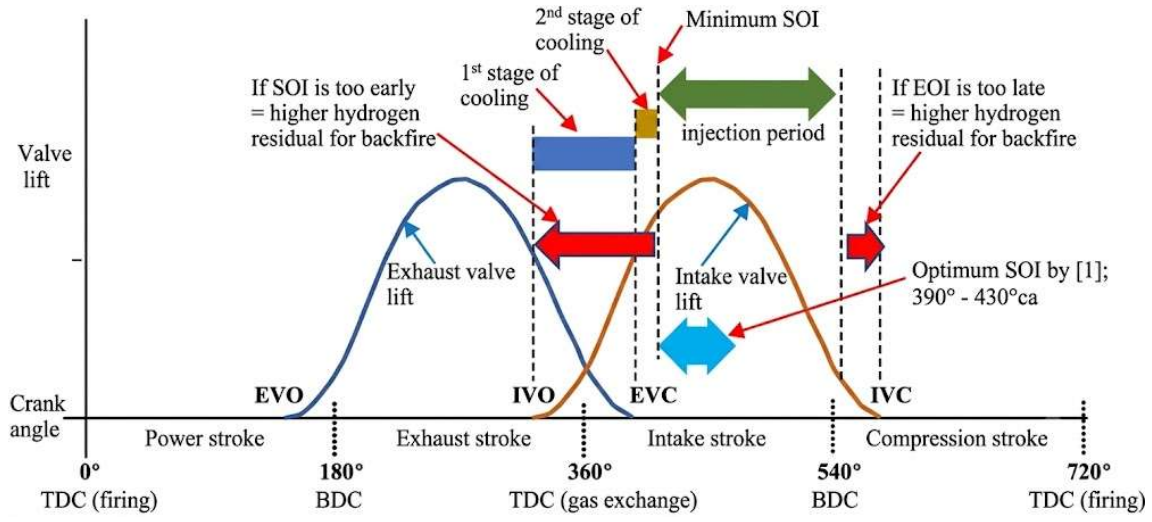


Figure 9. Backfire control strategy by adjusting hydrogen injection timing [12].

A comprehensive comparison of representative investigations evaluating hydrogen injection strategies, start of injection timings, and mixture preparation outcomes is summarized in Table 3 [14–16,24,25].

Table 3. Mixture formation characteristics and injection strategies in hydrogen engines.

Reference	Engine configuration/displacement	Fuel delivery/injection strategy	Key injection parameters (SOI, EOI, Pinj)	Main findings and conclusions
Gao et al. [10]	Single-cylinder/ multi-cylinder PFI SI engines	PFI	Optimized SOI: 390°–430° CA; injection pressure < 0.5 MPa	Early SOI increases fuel residence time in the intake runner, escalating backfire risk; delayed EOI leaves uninduced residual H_2 in the manifold, causing backfire in subsequent cycles.
Khalid et al. [12]	Automotive PFI hydrogen engine	PFI with injection timing control	Injection window coordinated within the IVO-IVC period	Establishing an optimum injection timing window avoids charge accumulation in the intake port and suppresses backfire without imposing significant volumetric efficiency penalties.
Yun et al.[13]	Single-cylinder SI engine	PFI	Multi-objective optimization for SOI and ST	Synchronous optimization of injection and spark timing effectively prevents localized hydrogen accumulation near the intake valve seat and enhances indicated efficiency.
Lu et al.[23]	Single-cylinder hydrogen PFI research engine	PFI	Experimental sweeps for SOI from −450° to −210° CA ATDC. Classified backfire into Zones I, II, and III.	Identified safe Zone A (SOI between −430° and −360° CA ATDC) before IVO, achieving nearly backfire-free operation.
Kinkhabwala et al. [22]	Single-cylinder optical PFI engine	PFI	Experimental & 3D CFD simulation	3D CFD sweeps for SOI from 340° to 440° CA ATDC. Optimal SOI window identified between 380°–420° CA ATDC (20%–30% intake valve lift). Too early SOI leads to fuel bouncing back, while late SOI traps residual hydrogen near the intake valve, triggering backfire.
Musy et al. [4]	0.5 L single-cylinder research engine	PFI vs. DI comparison	Single-hole, multi-hole (4, 6, 10 holes), and hollow-cone nozzles; P_{inj} = 0.2–1.0 MPa for PFI	Multi-hole nozzle geometries induce smaller high-frequency turbulent eddies and faster dissipation rates, achieving superior fuel–air homogenization compared to hollow-cone configurations.
Zhang et al. [40]	Single-cylinder	SI Ammonia Engine operating with On board Exhaust Fuel Reforming	3D CFD numerical study with detailed chemical kinetics NH_3 and $H_2$for exhaust fuel reforming	H_2 rich reformate gas accelerates flame propagation, elevates P_{max} and HRR_{max}, drastically cuts unburned NH_3 slip, but increases NO_x due to higher peak combustion temperatures.

4. Combustion dynamics and abnormal combustion phenomena

4.1. Ignition initiation, flame kernel development, and detailed kinetic mechanisms

Ignition initiation and early flame development in hydrogen internal combustion engines diverge fundamentally from conventional hydrocarbon combustion, exhibiting markedly accelerated kinetics and distinct morphological evolution. In the initial kernel formation phase, the minimal energy required to trigger self-sustaining flame kernels ensures reliable cold-start behavior and broadens stable operation well into ultra-lean regimes. As a result, the ignition delay—defined as the interval from spark discharge to detectable heat release—is exceptionally short. Spark advance critically governs this initiation phase: premature ignition under low in-cylinder thermodynamic states delays kernel propagation, whereas optimal spark retardation can optimize thermal efficiency while suppressing knock propensity. The in-cylinder combustion evolution is conventionally quantified using the MFB metric, typically demarcated into two distinct phases. The flame initiation stage, defined as the crank angle interval required to consume the initial 10% of the fuel-air mass, is predominantly dictated by early flame kernel development and ignition stability [10].

As characterized in the optical constant-volume bomb (Figure 10), flame propagation progresses through well-defined morphological transitions: initial kernel generation (A1), quasi-steady spherical expansion (A2–A3), onset and multiplication of cellular structures on the front (A4), and eventual stabilization of a fully developed cellular regime (A5). During early outward propagation, the flame front maintains a smooth, laminar structure with negligible local strain perturbations. Over time, intrinsic flame instabilities induce fine-scale surface wrinkling that subsequently transitions into coherent cellular networks. This morphological transformation indicates the onset of hydrodynamic and thermo-diffusive instabilities, effectively accelerating the transition from laminar spread to turbulent flame acceleration [17].

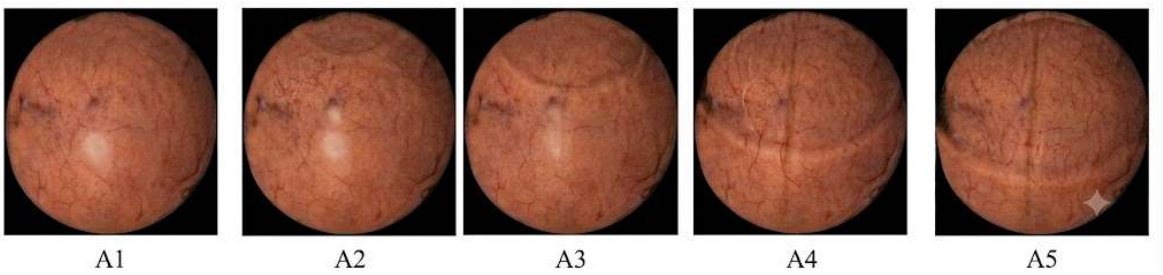


Figure 10. Partial schlieren image of a hydrogen-air mixture [17].

A detailed kinetic mechanism fully describes the hydrogen oxidation process through a network of elementary chemical reactions among reactants (H_2, O_2), products (H_2O), and intermediate radicals (H, O, OH, HO_2, H_2O_2) [41]:

Chain initiation: Initiated by the high-temperature thermal dissociation of H_2 molecules via binary collisions to generate H radicals:

$$H_2 + M \leftrightharpoons H + H + M$$

where M is a third body such as N_2, Ar, or He.

Chain branching: These are the most critical reactions that exponentially multiply radical concentrations and drive the overall reaction rate:

$$H + O_2 \leftrightharpoons O + OH$$

$$O + H_2 \leftrightharpoons H + OH$$

Chain propagation:

$$OH + H_2 \leftrightharpoons H_2O + H$$

HO_2/H_2O_2 formation and consumption (at high pressure and intermediate temperature): under elevated pressures, recombination producing HO_2 competes with the chain-branching pathway [26]:

$$H + O_2 + M \leftrightharpoons HO_2 + M$$

$$HO_2 + H \leftrightharpoons OH + OH$$

$$HO_2 + HO_2 \leftrightharpoons H_2O_2 + O_2$$

$$H_2O_2 + M \leftrightharpoons 2OH + M$$

Several detailed mechanisms are standard in combustion modeling: the Mueller/Dryer mechanism (19 reversible reactions calibrated over 850–1040 K) [17], the Ó Conaire model (10 species and 19 reactions, highly popular in engine simulations), and the comprehensive framework [41]. For specialized high-pressure modeling and termolecular pathways, researchers utilize the expanded Konnov mechanism (28–33 steps) [26], while the hydrogen sub-model of GRI-Mech 3.0 serves as a widely referenced baseline for fundamental H_2/O_2 kinetics [17].

4.2. Flame propagation and heat release rates

The coupled relationship between turbulent flame propagation and HRR constitutes the governing mechanism behind the thermodynamic behavior of hydrogen-fueled engines. As demonstrated in Figure 11, the rapid consumption of the air-hydrogen mixture during Stage II premixed combustion induces steep pressure gradients immediately following top dead center, while increasing engine rotational speed from 1500 to 4000 rpm attenuates the peak pressure rise rate PRR_{max} from over 3.6 to below 2.0 bar/° CA due to physical residence-time compression per crank angle degree [42]. Concurrently, the experimental findings in Figure 12 establish that advancing engine load from 3.7 to 10.7 bar BMEP at 2000 rpm drives peak heat release rate from roughly 34 to nearly 88 J/° CA, thereby elevating peak combustion temperatures from 1507 K to beyond 1630 K [42]. Consequently, while heightened flame velocities facilitate rapid isometric heat addition and enhance indicated thermal efficiency, the accompanying escalation in HRR_{max} and localized in-cylinder thermal fields at elevated loads intensifies thermal stress and amplifies both pre-ignition tendencies and NO_x synthesis, underscoring the critical need for precise spark timing, mixture stratification, or exhaust gas recirculation strategies.

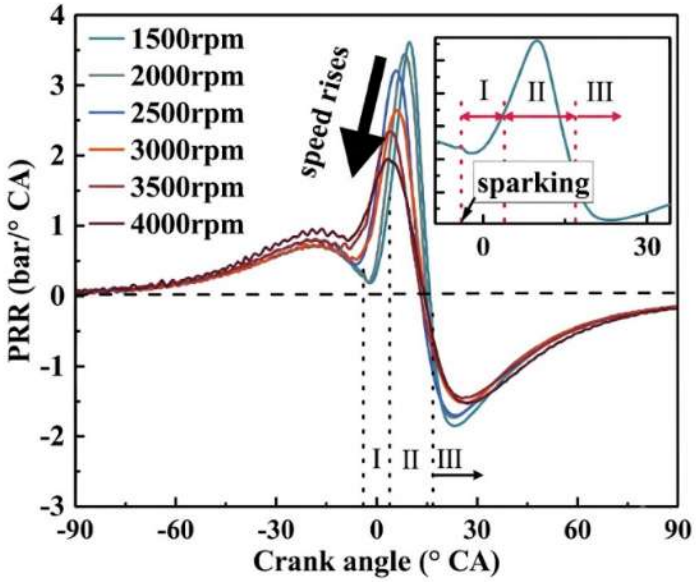


Figure 11. PRR with crank angle at different engine speeds at BMEP = 10 bar [42].

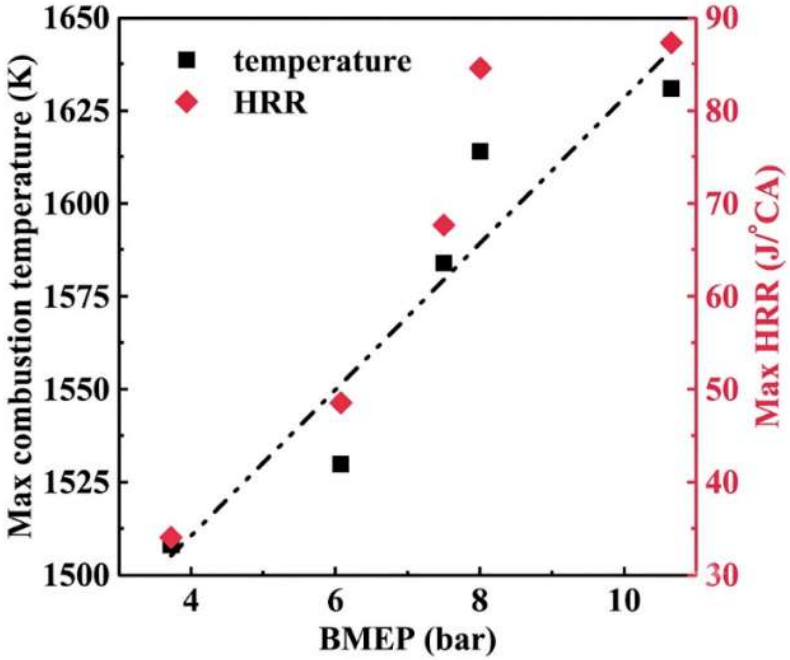


Figure 12. Maximum combustion temperature and maximum HRR with BMEP at 2000 rpm [42].

4.3. Cyclic dispersion and combustion stability

Characterizing combustion stability in hydrogen internal combustion engines is paramount for maximizing indicated thermal efficiency and securing operational robustness. Stability reflects the deterministic and stochastic reproducibility of the in-cylinder thermochemical heat release across successive operating cycles, constraining energy conversion within optimal crank-angle windows while precluding abnormal combustion phenomena, including misfire, backfire, and stochastic pre-ignition. This cyclic consistency is standardly quantified via statistical metrics of cycle-to-cycle variability; predominantly, the coefficient of variation of indicated mean effective pressure [24].

In hydrogen engines, cyclic stability is governed by mixture preparation dynamics and ignition parameters. Operating in ultra-lean regimes amplifies cycle-to-cycle variations and drives up COVIMEP, thereby deteriorating combustion stability. Consequently, precise coordination between ST and SOI is imperative: optimal timing promotes charge homogeneity and sustained flame kernel development, whereas extreme spark advance or delay, as well as delayed injection phasing, degrades stability through poor charge preparation and erratic heat release [30]. In direct-injection architectures, EDI demonstrates superior cyclic stability over LDI by enabling a more dispersed, homogeneous in-cylinder charge [15]. In a hydrogen engine under DI plus lean-burn mode, the ideal mixture stratification law is that the gas fuel concentration is gradually stratified from the ignition center to the periphery region [43]. While abnormal combustion modes, such as knock, exacerbate cyclic fluctuations, advanced ignition strategies—notably, TJI—effectively stabilize the combustion process by accelerating early flame propagation. Conversely, co-firing with ammonia compromises cyclic stability due to its lower chemical reactivity and suppressed laminar burning velocity.

4.4. Mechanisms of abnormal combustion

4.4.1. Intake backfire

Backfire in port fuel injection hydrogen internal combustion engines is triggered when a combustible in-manifold mixture interacts with an active thermal or electrical source [44]. The primary thermal triggers include in-cylinder localized hot spots—such as overheated spark plug electrodes, exhaust valves, cylinder walls, and lubricating oil-derived carbon deposits—as well as the backflow of hot residual gases into the intake runner during the valve overlap period [44]. Furthermore, persistent flame kernels carried over from prior compression-stroke pre-ignition, prolonged combustion, severe knock, or misfire events can directly ignite the fresh incoming charge upon IVO. Beyond combustion chamber anomalies, external thermal sources such as actively heated intake sensors (e.g., intake-mounted UEGO sensors) and ignition system malfunctions—notably parasitic spark discharge driven by residual inductive energy in the ignition coils during the intake stroke—also serve as direct backfire initiators.

Figure 13 demonstrates the backfire mechanisms where the fresh mixture is ignited either via pre-ignition inside the cylinder spreading upstream or through direct contact with backflowing hot exhaust gases in the intake manifold [2]. The propensity for backfire is heavily dictated by the fuel delivery schedule and engine operating boundaries. In Figure 14, parametric investigations identified three critical SOI risk regimes: Zone I: SOI < −430° CA ATDC, where premature injection induces fuel accumulation behind the closed intake valve that ignites upon encountering residual gases at IVO; Zone II: −360° CA < SOI < −280° CA ATDC, where injection proceeds shortly after IVO before fresh intake air can adequately cool in-cylinder hot spots; and Zone III (EOI > −270° CA or beyond −190° CA ATDC), where incomplete fuel induction prior to IVC leaves residual hydrogen in the intake tract for the subsequent cycle. Operationally, backfire is most pronounced under high-load or near-stoichiometric conditions ($\lambda = 1$), where elevated combustion temperatures drive up component surface thermal loading, as well as at low engine speeds, which markedly prolong the contact residence time between the incoming mixture and hot residual gases.

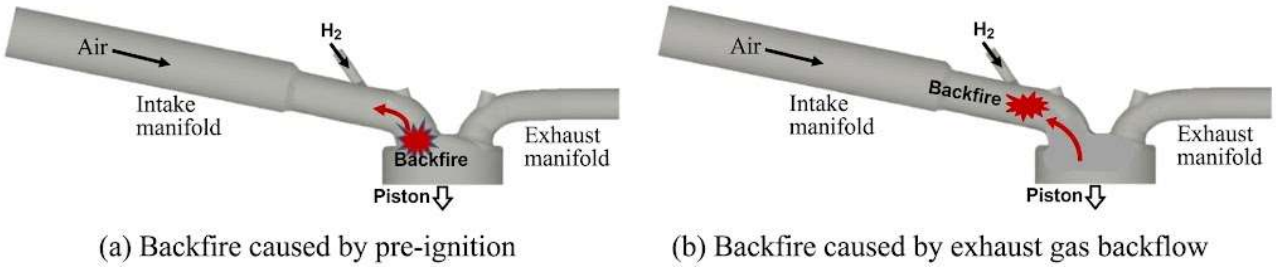


Figure 13. Backfire caused by pre-ignition and residual exhaust gas backflow, reproduced from [2].

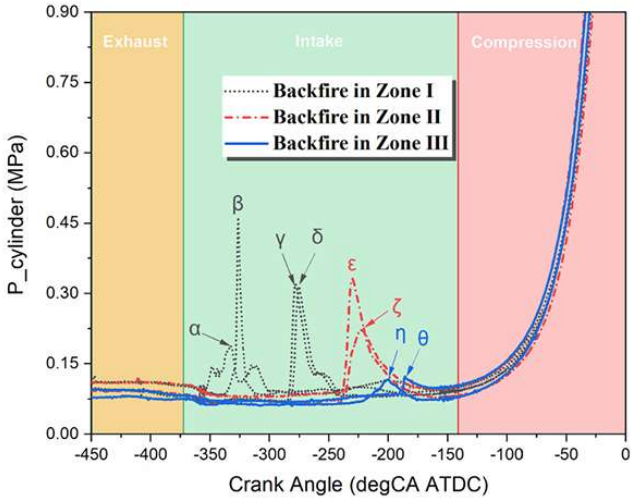


Figure 14. Cylinder transient pressure in different zones when backfire occurs [2].

Abnormal combustion remains one of the most critical challenges limiting the performance, efficiency, and operating range of hydrogen internal combustion engines. Owing to hydrogen's unique physicochemical properties, including its low ignition energy, wide flammability limits, and high laminar flame speed, H2ICE is highly susceptible to combustion anomalies such as backfire, pre-ignition, and knock.

In Figure 15, backfire is particularly prevalent in PFI systems, where the premixed hydrogen-air charge in the intake manifold is ignited by hot residual gases, overheated spark plugs, or exhaust valve hot spots [44,45].

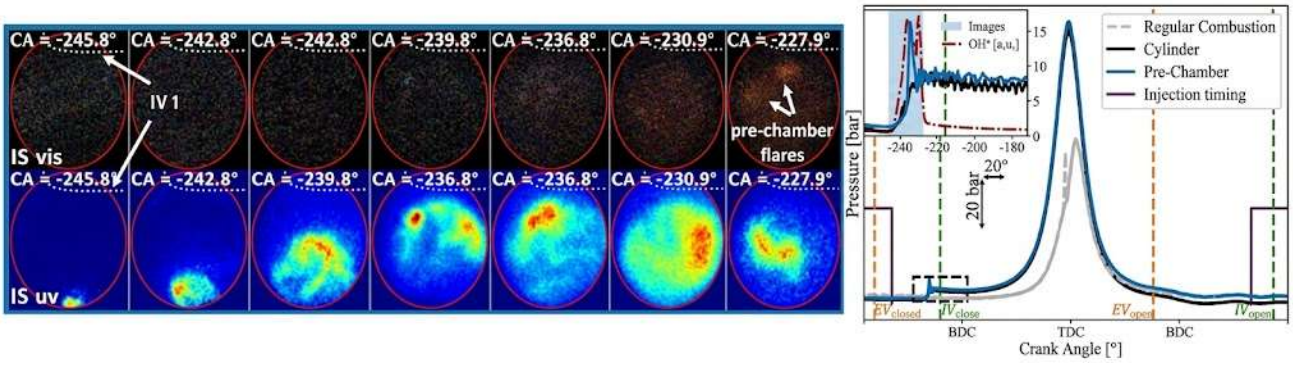


Figure 15. Early backfire during fully open intake valves [45].

In Figure 16, pre-ignition occurs when the mixture ignites before the scheduled spark event, typically triggered by combustion-chamber hot spots or thermally decomposed lubricating-oil droplets, resulting in an excessive pressure rise BTDC [3,17,23,45].

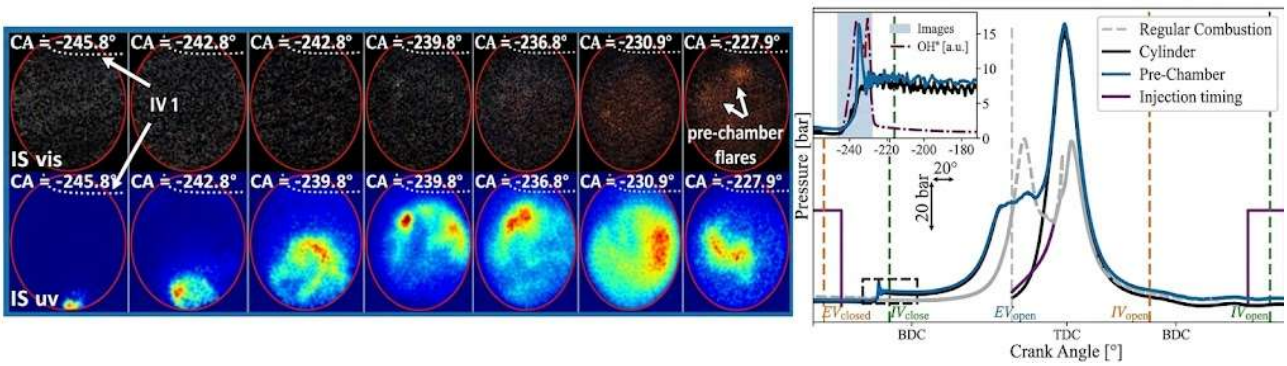


Figure 16. Late backfire while the intake valves are almost closed. Flame development in the OH* radical emissions spectrum [45].

The proper delay of the fuel injection decreased the intensity of backfire due to an increased cooling duration of residual exhaust gas by fresh intake air, as shown in Figure 17. The backfire intensity was decreased by delaying ignition timing, and it disappeared when the ignition timing was later than 14° CA BTDC. Additionally, the backfire occurrences were advanced by delaying ignition timing; when ignition timing was earlier than 14° CA BTDC, backfire occurred around 45° CA BTDC [10].

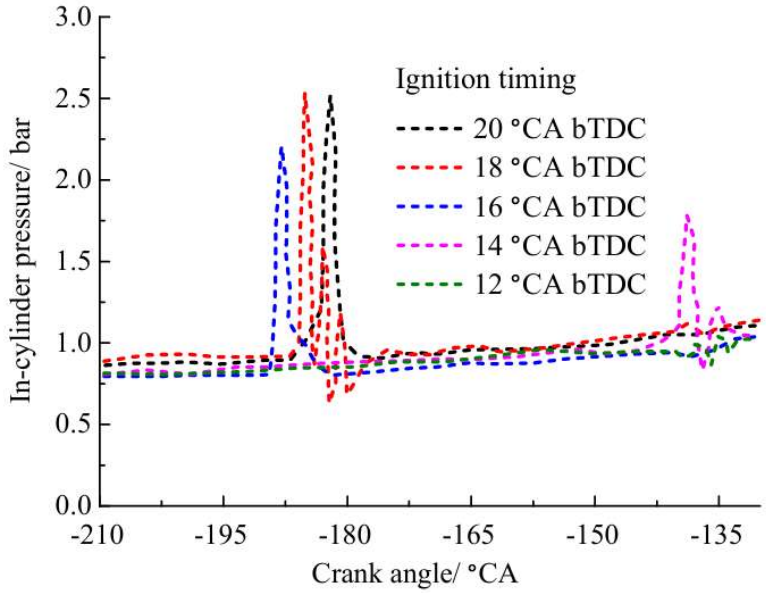


Figure 17. Backfire caused by improper ignition timing under the fuel-air equivalence ratio of 0.82. Hydrogen-air equivalence ratio, 0.82; intake valve opening, 3.5° CA BTDC; intake valve closing 81.5° CA aBDC; TDC, 180° CA [10].

At the operational level, optimizing the fuel injection strategy serves as the primary safeguard against backfire in PFI architectures. Delaying the SOI allows unthrottled, clean intake air to enter the cylinder during the early intake stroke, establishing a pre-cooling effect that scavenges hot residual gases and cools in-cylinder hot spots prior to fuel admission. Defining an optimized injection window—specifically

maintaining SOI within a verified safe zone such as −430° to −360° CA ATDC (or 390° to 430° CA, depending on intake runner geometry)—effectively suppresses backfire propensity while retaining adequate residence time for mixture homogenization. Concurrently, advancing the EOI ensures the injection event terminates well before IVC, eliminating residual hydrogen pooling along the intake runner walls. These injection protocols are reinforced through injector hardware enhancements. Directing injector nozzles toward the intake valve seat and positioning injectors in close proximity to the valve face minimizes wall impingement and fuel residence time in the manifold. The adoption of dual-injector arrangements and elevated injection pressures promotes supersonic jet penetration and accelerated turbulent mixing, preventing localized hydrogen-rich pockets that can trigger early ignition.

To control in-cylinder thermal thresholds, charge dilution and active cooling methods provide robust suppression. Introducing 12%–25% cooled EGR lowers both the laminar flame speed and peak cycle temperatures, curtailing backfire frequency by over 50%. Similarly, intake WI exploits water's high latent heat of vaporization to rapidly quench localized hot spots and suppress premature reaction kinetics [46]. Thermal management is further coupled with valvetrain and ignition system adjustments. Minimizing valve overlap duration via VVT restricts high-temperature exhaust blowback into the intake tract during gas exchange [46,47]. Thermal mitigation of persistent hot spots relies on cold-rated or water-cooled spark plugs to accelerate electrode heat dissipation [44], alongside sodium-cooled exhaust valves and redesigned cylinder head coolant jackets [46].

Finally, passive arresters and closed-loop control architectures furnish vital fail-safe capabilities. Wire-mesh flame arresters situated within the intake runner act as physical heat sinks that quench propagating flame fronts, safeguarding upstream components against structural damage [1,48]. Concurrently, adaptive ECU strategies dynamically monitor critical thermal states, including lubricant temperatures. Upon crossing calibrated thresholds, the ECU automatically delays the injection timing (40° CA ATDC), inducing thermal quenching and averting imminent backfire events [44].

4.4.2. Pre-ignition

Pre-ignition in H_2ICE is primarily classified into two distinct modes based on initiation timing and in-cylinder pressure characteristics: PEMC (170° to 80° CA BTDC) and PLC (near TDC) in Figure 18 [49]. PEMC is characterized by an abrupt in-cylinder pressure rise with peak pressures consistently converging at TDC, predominantly occurring under torque outputs of 70 ÷ 100 Nm and ultra-lean conditions (λ = 1.5 ÷ 3.3). Conversely, PLC manifests late in the compression stroke and exhibits high-frequency pressure oscillations analogous to super-knock [49]. This phenomenon is driven by complex thermodynamic interactions, predominantly combustion-chamber hot spots—such as spark plug electrodes, exhaust valve heads, or carbon deposits—exceeding the auto-ignition threshold of hydrogen (858–950 K) [50]. The relative impact of hotspot characteristics follows the order contact area > initial temperature > heating rate > residence time [50]. Additionally, lube-oil pyrolysis generating suspended incandescent droplets (the HyLube mechanism), elevated residual gas temperatures, high-load and low-speed operation, and stoichiometric mixtures (λ approximately 1) substantially amplify pre-ignition propensity [3,49].

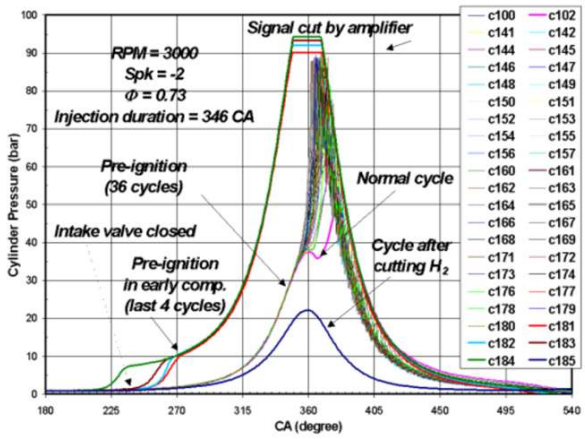


Figure 18. In-cylinder pressure of preignition on the Ford P2000 hydrogen engine [49].

The ramifications of pre-ignition severely undermine engine performance, structural durability, and emission levels. Premature combustion generates negative compression work against the ascending piston, causing reductions in BP and BTE in 93.1% and 91.5% of documented cases, respectively [49]. Concurrently, elevated localized peak temperatures drive an abrupt surge in NO_x emissions across 77.2% of occurrences [49]. More critically, cumulative thermal build-up can induce runaway pre-ignition, progressively advancing combustion initiation (from −25° CA to −30° CA) and exerting destructive mechanical loads that risk catastrophic engine failure [28,46]. Furthermore, if the pre-ignition flame kernel persists until IVO, it ignites the incoming fresh charge, triggering severe backfire into the intake manifold [17]. Figure 19 lists the importance of all input features on the impact of PEMC events. For all input features, injection timing consistently obtained the highest importance [48].

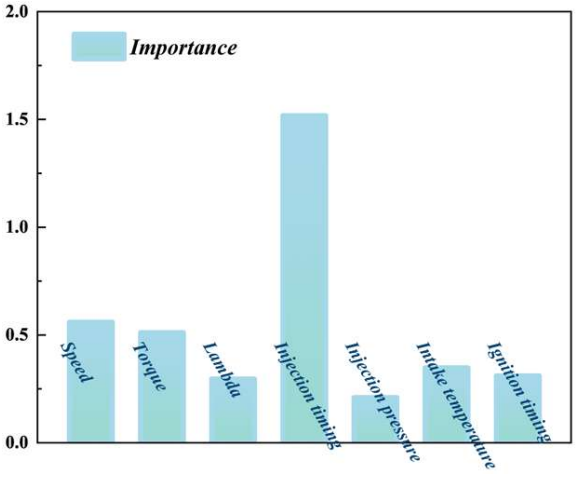


Figure 19. Importance of input features in PEMC events [48].

Mitigating and suppressing pre-ignition requires a synergistic combination of injection calibration, thermal moderation, and structural optimization. Adjusting the SOI is pivotal: Delaying SOI beyond 180° CA BTDC in HDI configurations eliminates PEMC events, whereas maintaining SOI within −430° to −360° CA ATDC in PFI systems ensures a preliminary air-scavenging phase that cools hot spots before hydrogen admission [49]. Simultaneously, thermal dilution via cooled EGR or manifold WI effectively attenuates peak cycle temperatures and quenches thermal hot spots [47]. Structural countermeasures include utilizing platinum-free cold-rated spark plugs, sodium-cooled

exhaust valves, optimized cylinder-head cooling passages, and disk-shaped combustion chambers to minimize localized turbulence, as well as adopting low-ash lubricants paired with upgraded piston rings to curb oil ingress [27]. Finally, deploying predictive machine learning frameworks—particularly RF classifiers achieving prediction accuracies of 97.69%–98.76%—offers an effective pathway toward closed-loop, real-time ECU mitigation of pre-ignition hazards [49].

4.4.3. Knock, super-knock, and fast flame propagation

Conventional knock in hydrogen internal combustion engines refers to the spontaneous auto-ignition of the unburned end-gas charge ahead of the advancing primary flame front [51]. Driven by high chemical reactivity, the trapped end-gas undergoes intense compressive heating and densification by the propagating flame, triggering rapid exothermic kinetics and localized thermal runaway [51,52]. Notably, knock in hydrogen-fueled engines exhibits a dual nature comprising heavy knock and light knock: Heavy knock originates from the explosive auto-ignition of the bulk end-gas, generating steep shock waves that impinge upon the chamber walls to induce severe high-frequency pressure oscillations and metallic acoustic signatures [1], whereas light knock stems from combustion instability induced phenomena, where the unstable propagation of the high-velocity flame front emits radial pressure waves that undergo acoustic superposition off the cylinder walls to produce discernible knocking noise even without macroscopic end-gas auto-ignition [53]. In Figure 20, conventional knock is diagnostically characterized by KI or MAPO values typically ranging from 0.1 to 0.3 MPa (1–3 bar) [41], with the corresponding HRR profiles characteristically displaying a distinctive two-peak combustion pattern [51].

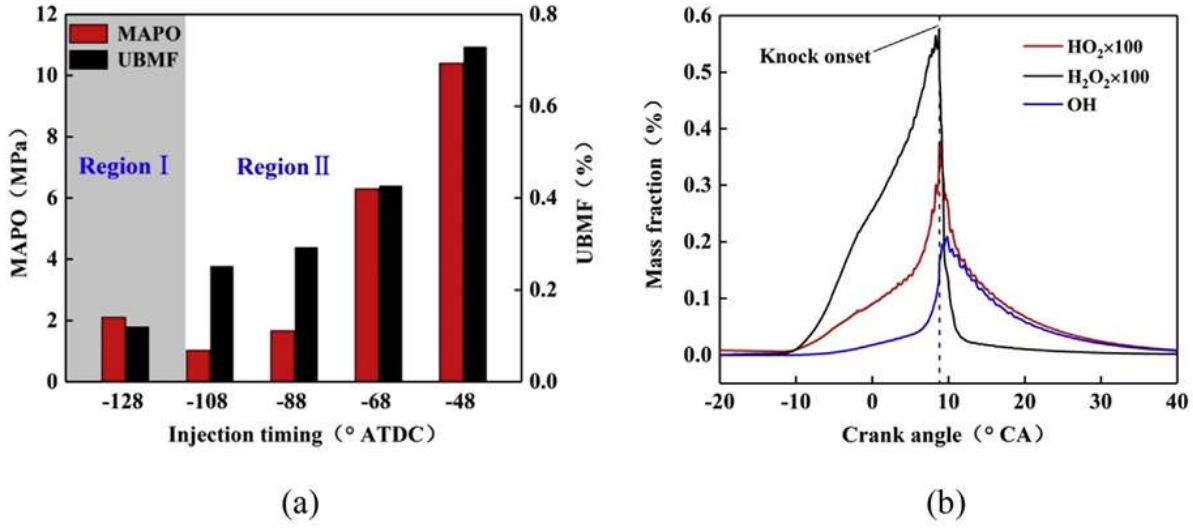


Figure 20. (a) MAPO and UBMF under different injection timings and (b) chemical species mass fraction during knock combustion under an SOI of −68° ATDC [41].

Super-knock represents an exceptionally destructive abnormal combustion phenomenon characterized by pressure oscillation amplitudes or KI that exceed conventional knock thresholds by 1–2 orders of magnitude, typically yielding KI > 3 MPa or MAPO spanning from 30 to over 100 bar [51,53] (In Figure 21). Mechanistically, super-knock is driven by the deflagration-to-detonation transition or the tight coherent coupling between a supersonic shock front and the chemical reaction front, resulting in a developing detonation wave [51,53]. Strong compressive shock waves emitted by

the primary flame front compress the unburned near-wall charge, accelerating intermediate kinetic pathways and prompting extensive chemical precursor accumulation [19]. Consequently, massive multi-point auto-ignition triggers explosive detonation waves that interact constructively with the flame front to consume the remaining unburned mixture within an extremely narrow crank angle window of approximately 1.8° CA [51].

This regime is strongly correlated with, and frequently precipitated by, preceding pre-ignition events or in-cylinder localized hot spots [17]. Furthermore, super-knock propensity exhibits profound sensitivity to the engine CR; experimental investigations on CFR engines demonstrate that elevating the CR from 8.5 to 10.0 exponentially increases the occurrence frequency of super-knock cycles from 0.4% to 45% [53]. In terms of HRR characteristics, super-knock profiles display multi-peak sharp oscillations followed by an abrupt cessation, reflecting the quasi-instantaneous consumption of the bulk in-cylinder charge [51].

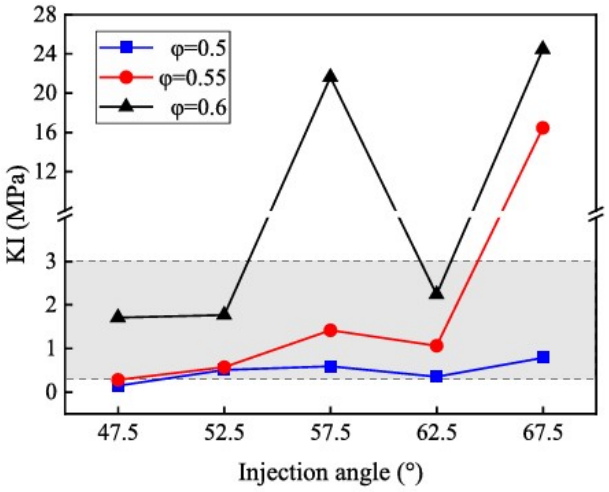


Figure 21. Variation of KI with injection angles at different equivalence ratios [50].

Fast flame propagation represents a distinct combustion regime in hydrogen internal combustion engines, characterized by the ultra-rapid propagation of the spark-ignited flame front across the combustion chamber, which induces substantial pressure oscillations and audible knocking noise completely in the absence of macroscopic end-gas auto-ignition [53]. Physically, owing to the intrinsically high laminar burning velocity of hydrogen relative to conventional hydrocarbon fuels [54] operations under low compression ratios and near-stoichiometric mixtures cause the flame front to expand at an extreme velocity, triggering sharp escalations in both the HRR and the pressure rise rate [54]. Consequently, this phenomenon is highly susceptible to being misdiagnosed as conventional auto-ignition knock when evaluated solely through acoustic sensors or in-cylinder pressure derivative signals on conventional metal engines [52]. Nonetheless, advanced optical diagnostics combined with 3D CFD simulations confirm that the flame front propagates continuously from the spark discharge without the formation of any isolated, discrete auto-ignition kernels within the unburned mixture [53].

4.5. Synthesis of combustion and stability studies

Table 4 synthesizes recent experimental and numerical findings on combustion phase development, cyclic stability indicators, and abnormal combustion phenomena across various engine configurations.

Table 4. Synthesis of combustion characteristics, stability, and abnormal combustion mitigation.

Reference	Operational mode/engine setup	Tested parameters (λ, ST, CR, load)	Abnormal combustion observed/investigated	Observed combustion behavior and mitigation outcome
Piano et al. [5]	0.5 L single-cylinder PFI engine	Over 45 operating conditions; tabulated laminar flame speed with polynomial correlation	Knock tendency under high-load intake conditions	Tabulated laminar burning velocity model achieved a combustion duration error < 3° CA across 45 operating conditions; accurately captured flame development and cyclic dispersion
Marwaha and Subramanian [21]	Single-cylinder automotive SI engine	PFI; equivalence ratio sweeps ($\phi = 0.3 \div 1.0$), varying engine speed and ignition timing	Backfire initiation, duration, and cycle termination	Mapped the backfire boundary, showing that backfire is heavily promoted at stoichiometric or near-rich mixtures and suppressed by charge lean-up and intake component temperature reduction
Rao et al. [24]	Multi-cylinder PFI hydrogen engine	Multi-objective optimization: load (BMEP 4–10.5 bar), ST sweeps, engine speeds 1500–4000 rpm	Peak pressure rise rate, heavy knock, and pre-ignition	Peak combustion temperature and maximum HRR increased linearly with BMEP (from 1505 K to 1630 K, HRR from 34 to 87 J/° CA at 2000 rpm); identified optimal ST to balance thermal efficiency and knock
Deist et al. [45]	Medium-speed maritime hydrogen engine	Large-bore configuration with endoscopic optical access	Endoscopic visualization of early and late backfire through intake valves	Backfire initiates around the hot intake valve seat during early IVO or late IVC; captured backward OH* radical chemiluminescence propagation into the intake runner
Dhyani and Subramanian [44]	Automotive PFI hydrogen engine	Closed-loop electronic control unit with real-time feedback	Manifold backfire and flame propagation into intake	Developed an online control strategy that instantly eliminates backfire through real-time transient injection cutoff and dynamic spark timing adjustments
Manzoor et al. [53]	3D numerical model (SI hydrogen engine)	Detailed kinetic mechanisms; stoichiometric to lean mixtures	Fast flame propagation, deflagration-to-detonation transition (DDT), super-knock	Captured distinct abnormal combustion modes and localized pressure oscillations resulting from rapid end-gas auto-ignition and supersonic flame front coupling

5. Influence of engine design and operating parameters

5.1. Injection phasing and strategy

The precise phasing of the SOI and EOI governs both in-cylinder hydrogen trapping efficiency and the mitigation of backfire. Optimal hydrogen delivery (typically observed at an SOI between 380° CA and 430° CA) occurs when the intake valve reaches 20%–30% of its maximum lift, allowing the high-velocity intake airflow to effectively entrain the gaseous hydrogen directly into the combustion chamber. Conversely, premature injection (early SOI) before adequate valve opening induces backflow into the intake runner or plenum, while delayed injection (late EOI) leaves insufficient residence time before IVC, resulting in incomplete induction and compromised in-cylinder fuel mass. Mechanistically, backfire propensity is dictated by these boundary timings: An overly advanced SOI permits hydrogen accumulation adjacent to the intake valve seat, which ignites upon IVO through exposure to hot residual gases or combustion chamber hot spots (Zone I). Symmetrically, an excessively delayed EOI leaves unburned residual hydrogen within the intake port post-IVC, priming premature ignition during the subsequent cycle's intake stroke. Consequently, establishing an optimized injection window (SOI between 390° CA and 430° CA or from −430° CA to −360° CA ATDC) eliminates backfire by utilizing initial pure intake air to pre-cool thermal hot spots while guaranteeing complete scavenging of hydrogen into the cylinder prior to IVC.

Elevating injection pressure and deploying multiple-injection strategies provide robust mechanisms for enhancing mixture homogeneity and suppressing abnormal combustion. Higher injection pressures augment jet momentum, penetration depth, and turbulent kinetic energy, which substantially compress the required injection duration or pulse width [55]. This temporal compression establishes a vital safety buffer between EOI and IVC, ensuring thorough mixture induction, preventing intake-port fuel pooling, and effectively curbing pre-ignition and backfire; in DI architectures, high-pressure fueling post-IVC entirely eliminates hydrogen from the intake manifold, inherently mitigating backfire risk. Complementing pressure optimization, split-injection strategies (such as spatially or temporally separated pulses) enable precise spatio-temporal regulation of the in-cylinder equivalence ratio. By eliminating fuel-rich local pockets and moderating the peak heat release rate, split injection substantially suppresses thermal NO_x formation and mitigates the severe intake air displacement penalty common to PFI configurations, thereby elevating volumetric charging efficiency, stabilizing cyclic variations, and systematically quelling knock and pre-ignition [14].

5.2. Combustion phasing and equivalence ratio

Spark timing fundamentally dictates the combustion phasing trajectory, directly modulating in-cylinder pressure and temperature evolution. Advancing spark timing toward the MBT threshold sharpens the HRR, elevates peak in-cylinder pressure, and accelerates overall combustion kinetics, thereby conferring substantial enhancements in IMEP and BTE [52]. However, excessive spark advancement triggers premature pressure accumulation prior to TDC, incurring severe negative compression work penalties while dramatically compounding susceptibility to abnormal combustion anomalies, specifically engine knock and pre-ignition. Conversely, retarding spark discharge toward or beyond TDC shifts primary heat release deeper into the expansion stroke, which curtails peak chamber pressures and temperatures at the expense of marginal compromises in mechanical power output and thermal efficiency [17].

From an emissions perspective, spark timing constitutes a pivotal calibration lever for regulating NO_x formation, which operates almost exclusively via the thermal Zeldovich mechanism at

temperatures exceeding 1800 K within hydrogen-air mixtures. Advancing the ignition timing elevates localized combustion temperatures into the thermal NO_x generation threshold, prompting an exponential surge in exhaust emissions. In contrast, strategically delaying the spark timing lowers peak localized reaction zone temperatures, serving as an extraordinarily robust, non-intrusive mitigation pathway to suppress thermal NO_x formation by orders of magnitude without requiring dilution recalibration or alterations to the base fuel-air equivalence ratio [17].

Combustion phasing parameters play a critical role in determining the efficiency, power output, emissions, and combustion stability of H2ICEs. In Figure 22, ST is the primary means of controlling combustion phasing and is typically optimized using the CA50 location [36].

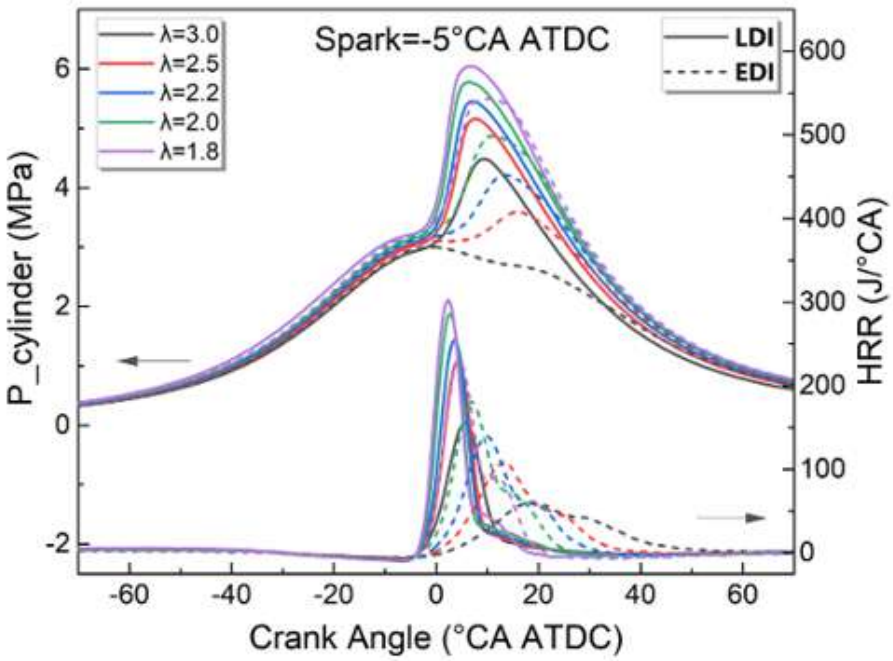


Figure 22. Cylinder pressure and HRR of LDI and EDI under different spark timing [36].

Excessive spark advance escalates cylinder-wall and spark-plug electrode temperatures, promoting the formation of localized hot spots that can serve as nucleation sites for backfire in subsequent cycles. Conversely, over-delaying the spark timing significantly elevates EGT due to late-phase combustion extending into the expansio stroke [43]. Once the EGT surpasses the critical threshold (540 °C), hot residual gases, particularly during the valve overlap period, can readily trigger backfire events. Consequently, spark timing must be synergistically co-optimized with the hydrogen SOI to concurrently suppress engine knock and backfire [17]. In Figure 23, λ and ST are key parameters, with lean-burn operation enhancing thermal efficiency and substantially reducing NO_x emissions by lowering combustion temperatures; however, excessively lean mixtures can increase cycle-to-cycle variations and misfire tendencies [5,24,27].

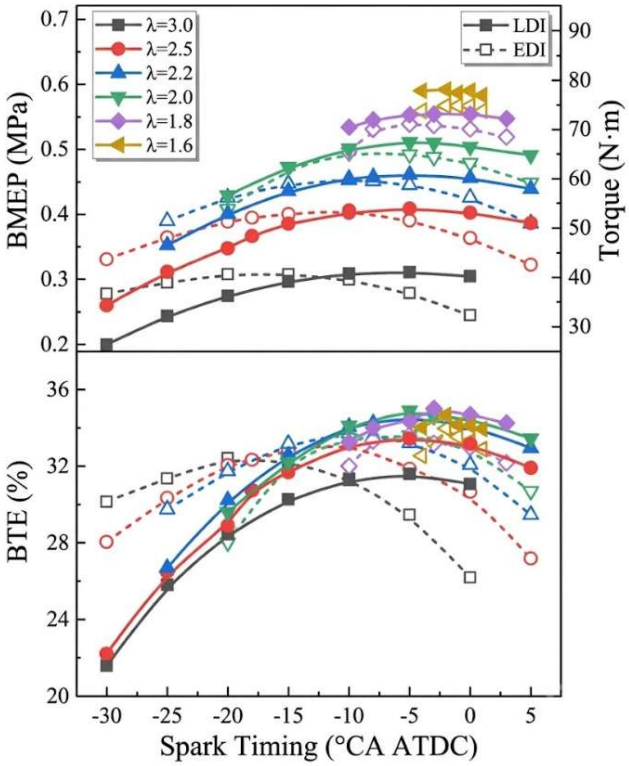


Figure 23. BMEP and BTE of LDI and EDI under different spark timings [36].

5.3. Engine structural parameters

Engine design and operating conditions play a pivotal role in managing the unique combustion characteristics of hydrogen, particularly its high flame speed and low ignition energy, while balancing efficiency and emission targets.

Owing to hydrogen's elevated auto-ignition temperature (858 K) and superior RON > 130, hydrogen internal combustion engines can operate at significantly higher compression ratios than their gasoline counterparts, thereby directly enhancing indicated thermal efficiency and power output [1,18,38]. Furthermore, an elevated CR reduces the clearance volume, thereby decreasing the hot residual gas fraction and mitigating the risk of backfire in PFI configurations [10,27,32]. However, despite these thermodynamic advantages, higher CRs inherently induce elevated peak in-cylinder pressures and temperatures, creating a conducive environment for thermal NO_x formation and exacerbating the tendency for engine knock, particularly under near-stoichiometric conditions [32]. To address this trade-off, the current literature suggests an optimal CR range of 14.5:1 to 15.1 for H2ICEs, which maximizes overall efficiency before heat transfer losses and knock limits impose counterproductive effects [32].

Engine speed exerts a multifaceted and often contradictory influence on the combustion dynamics and operational stability of hydrogen internal combustion engines. Primarily, elevated engine speeds reduce the cycle duration available for heat dissipation, leading to higher exhaust gas temperatures that can thermally exacerbate backfire tendencies by heating the intake valves and manifold components [10]. Concurrently, increased rotational speeds enhance in-cylinder turbulence intensity, thereby significantly accelerating flame propagation [24]. This augmented internal flow introduces conflicting implications for overall stability: While extended injection durations in the crank angle domain can prevent localized hydrogen accumulation and thus reduce backfire risk in certain configurations, aggressive lean-burn strategies—often applied at high speeds to suppress further backfire—can

degrade combustion stability [23]. Consequently, such operational regimes frequently manifest as elevated cycle-to-cycle variations, quantified by a higher coefficient of variation in the indicated mean effective pressure.

Engine load profoundly dictates the thermal and mechanical operating boundaries of H2ICEs. High-load conditions inherently generate elevated peak in-cylinder pressures and temperatures, thereby exacerbating the engine's susceptibility to abnormal combustion phenomena such as pre-ignition, knock, and backfire [53]. From a thermodynamic perspective, BTE generally increases with increasing load, primarily because pumping and frictional losses constitute a diminishing proportion of the total work output [53]. Nevertheless, at extremely high-load regimes, this efficiency gain is frequently compromised; the mandatory implementation of delayed spark timing or advanced injection phasing to mitigate knock propensity often causes the BTE to plateau or precipitously decline [1,24]. Furthermore, the combustion of larger fuel quantities at high loads produces excessive peak temperatures, which invariably trigger a surge in thermal NO_x emissions. Consequently, sustainably managing high-load operations necessitates the integration of advanced mitigation strategies, most notably cooled EGR or lean-burn turbocharging (lean boosting), to simultaneously preserve mechanical integrity and ensure compliance with emissions regulations.

The inherent volumetric displacement of intake air by gaseous hydrogen—often termed the air displacement effect—necessitates turbocharging to recover and augment power density, thereby enhancing hydrogen dispersion and shortening combustion duration [30]. However, because elevated intake temperatures significantly increase the engine's vulnerability to pre-ignition and backfire, the integration of intercooling systems in boosted configurations is mandatory to maintain strict thermal safety margins [10,22]. Concurrently, excessive exhaust back pressure must be meticulously managed, as it induces internal exhaust gas recirculation, which traps high-temperature residual gases within the cylinder; the subsequent interaction between these hot residuals and the fresh combustible charge drastically increases the probability of backfire [45]. Finally, the geometric optimization of the intake manifold and the spatial configuration of the injectors are paramount to ensuring mixture homogeneity, as suboptimal architectures can create localized hydrogen-rich zones near intake valves, which serve as primary nucleation sites for backfire initiation [45].

6. Emission formation mechanisms and advanced mitigation strategies

6.1. Emission characteristics

Owing to the intrinsically carbon-free nature of hydrogen, the operation of port fuel injection hydrogen internal combustion engines inherently eliminates fuel-derived CO_2, CO, and HC at the tailpipe, thereby positioning NO_x as predominantly nitric oxide (NO), with minor fractions of NO_2 as the primary regulated exhaust pollutant [56]. Beyond NO_x, a comprehensive emission inventory for PFI H2ICE systems also encompasses lubricating oil-derived species and unburned hydrogen slip. Specifically, the thermal evaporation, pyrolysis, and partial oxidation of lubricating oil films across the cylinder liner and piston ring pack generate trace quantities of HC, CO, CO_2, and particulate matter [27], while unburned H_2 slip arises from mixture entrapment within top-land crevice volumes or incomplete reaction pathways near ultra-lean operational boundaries [27].

In hydrogen combustion, NO_x formation is governed by distinct chemical kinetic pathways modulated by local peak temperatures, pressures, equivalence ratios, and residence times.

In hydrogen internal combustion engines, the generation of NO_x is overwhelmingly dominated by the extended Zel'dovich thermal mechanism, which typically accounts for over 90%–95% of aggregate emissions under stoichiometric and moderately lean operating regimes [42]. This kinetic

route is governed by three reversible elementary reactions [42]:

$$O + N_2 \leftrightharpoons NO + N$$

$$N + O2 \leftrightharpoons NO + O$$

$$N + OH \leftrightharpoons NO + H$$

Because the reaction rate constants exhibit an exponential Arrhenius temperature dependency, the initiation step requires substantial activation energy to break the strong triple bond of molecular nitrogen, becoming kinetically active only when localized burned-gas temperatures surpass approximately 1800 K. Consequently, the high laminar burning velocity and elevated adiabatic flame temperature of hydrogen induce severe temperature excursions near stoichiometric mixtures (lambda approximately 1.0–1.3), provoking an exponential surge in thermal NO_x yield that routinely reaches 2000–5000 ppm [2].

Under ultra-lean or heavily diluted operational regimes where peak combustion temperatures are curtailed well below the 1800 K threshold, thermal NO_x production is largely frozen, allowing intermediate kinetic pathways—specifically, the NNH and N_2O routes—to become prominent and contribute up to 20%–25% of the total [57]:

$$N_2 + H \leftrightharpoons NNH$$

$$NNH + O \leftrightharpoons NO + NH$$

This route is particularly accelerated in hydrogen combustion due to the super-equilibrium pool of atomic hydrogen radicals characteristic of high-diffusivity hydrogen flames [57].

N_2O pathway: Proceeding through termolecular stabilization followed by radical attack:

$$O + N_2 + M \leftrightharpoons N_2O + M$$

$$N_2O + O \leftrightharpoons 2NO$$

$$N_2O + H \leftrightharpoons NO + NH$$

This mechanism gains kinetic prominence under lean, elevated in-cylinder pressures and high excess oxygen fractions.

The Fenimore mechanism requires carbon-containing radical species (predominantly CH and CH_2) to initiate the scission of atmospheric N_2 bonds, yielding precursor intermediates such as HCN and NH [17]. Because neat hydrogen contains no fuel-bound carbon, the prompt NO_x pathway is negligible in pure H2ICE.

Although hydrogen is a carbon-free fuel, minor traces of carbonaceous pollutants (HC, CO, and CO_2, alongside PM) are inevitably detected in the exhaust gas, primarily stemming from lubricating oil interaction. Hydrogen exhibits an exceptionally short quenching distance and high laminar burning velocity, which allow the flame front to propagate extremely close to the cylinder walls and piston crown crevices [27]. The resultant intense wall heat flux and thermal radiation induce localized evaporation and partial thermal oxidation of the oil film [27]. This phenomenon accounts for trace concentrations of HC, CO, and CO_2 (typically below 5–20 ppm), as well as PM emissions comprising unburned oil droplets and metallic ash additives. Simultaneously, unburned hydrogen slip remains a critical consideration [27]. The primary source of hydrogen slip is the fuel trapped within combustion chamber crevices—most notably the piston ring-pack crevices—during compression, effectively escaping the propagating flame front. Furthermore, under ultra-lean operating limits ($\lambda > 3.0$–3.5), the pronounced deterioration in flame speed exacerbates cyclic variations ($COV_{IMEP} > 5\%$), triggering partial misfires and flame quenching that can escalate unburned H_2 slip to levels as high as 1.2% by

volume in the exhaust manifold [57].

6.2. Advanced mitigation strategies in port hydrogen engines

In-cylinder thermal dilution serves as a primary pathway to decoupling high thermal efficiency from thermal NO_x generation. Exploiting the ultra-wide flammability limit of hydrogen, an ultra-lean burn strategy utilizes excess air as an effective heat sink, maintaining peak in-cylinder temperatures well below the 1800 K thermal Zel'dovich threshold and yielding single-digit engine-out NO_x concentrations (< 10 ppm) without intricate after-treatment dependencies [58]. Concurrently, cooled EGR at rates between 15% and 28% dilutes charge oxygen with inert N_2 and H_2O vapor [11]. In Figures 24 and 25, the implementation of cooled EGR at a 25% volume fraction can suppress NO_x formation by up to 57%, and when coupled with stratified direct injection under high-load conditions, these reductions can reach an impressive 84.4% [22]. Because the isobaric specific heat capacity of water vapor is considerably higher than that of dry air, this substitution elevates the overall charge heat capacity, dampens the laminar burning velocity, and curtails raw NO_x emissions by 75%–97% under high-load regimens while inherently suppressing pre-ignition and backfire. As a complementary thermal-sink approach, port WI leverages the superior latent heat of vaporization of water. At water-to-fuel mass ratios between 4:1 and 7.5:1, water atomization rapidly absorbs heat from intake air and hot spots, lowering peak thermal states and slashing NO_x formation by up to 97% [2].

Fine-tuning the transient mixture formation and ignition kinetics provides essential control over abnormal combustion phenomena and emissions. Regulating the SOI within an optimized window introduces an intake-air scavenge and pre-cooling phase for in-cylinder hot spots prior to hydrogen admission; this avoids the formation of localized fuel-rich zones, suppresses backfire propensity, and mitigates local thermal spikes responsible for NO_x formation [27]. Furthermore, spark timing retardation toward or slightly past TDC is utilized to shift the combustion phasing deeper into the expansion stroke. Although this introduces a marginal penalty in indicated thermal efficiency, the resultant drop in peak in-cylinder pressure and peak combustion temperature substantially curbs thermal NO kinetics during critical high-load excursions [11].

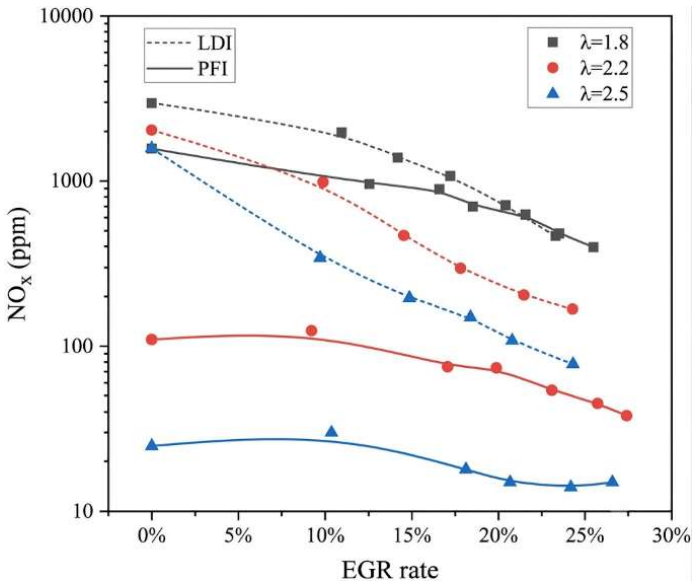


Figure 24. NO_X under different EGR rates, λ, and injection strategies [11].

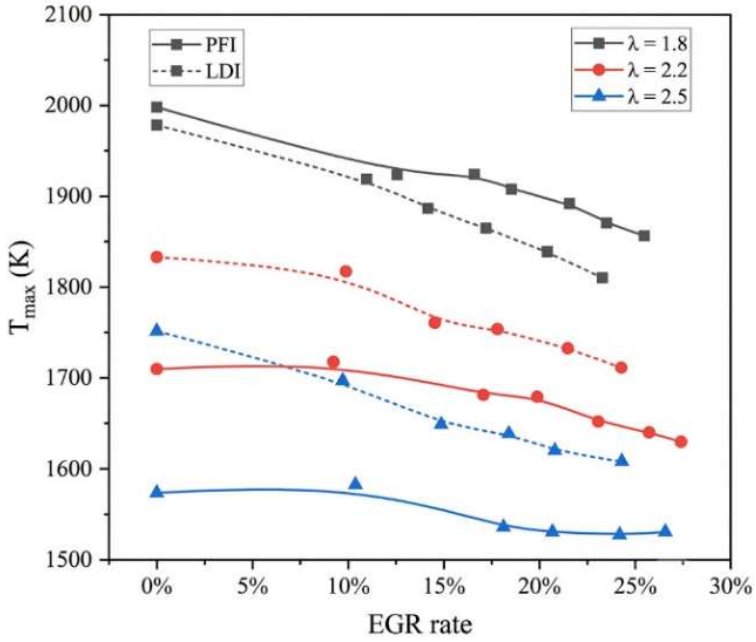


Figure 25. Tmax under different EGR rates, λ, and injection strategies [11].

To curtail oil-derived carbonaceous pollutants and minimize hydrogen entrapment, mechanical revisions and lubricant chemistry must be addressed concurrently. Formulations of low-viscosity, low-ash synthetic lubricants, when coupled with an optimized piston ring-pack tension and clearance profile, critically diminish oil film scraping variability, liner scuffing, and oil consumption. Limiting the oil mass exposed to the high-temperature flame front effectively suppresses the trace formation of carbonaceous species (HC, CO, and CO_2) as well as metallic ash PM [27]. Furthermore, integrating an active PCV system prevents the accumulation of blow-by hydrogen and entrained oil mist within the crankcase; this forced scavenging mitigates sub-surface fuel entrapment, lowers secondary oil-derived emissions, and preempts crankcase deflagration risks [49].

Under near-stoichiometric or moderately lean operation designed to maximize power density, in-cylinder mitigation must be supported by catalytic exhaust aftertreatment [56]. A hydrogen-assisted selective catalytic reduction architecture provides an elegant route by utilizing inherent engine-out H_2 slip directly as a non-toxic reducing agent over active catalysts to remediate NO_x. Alternatively, conventional urea-based NH_3-SCR systems remain capable of delivering sustained NO_x conversion efficiencies surpassing 90%–98% [59]. To counter residual reductant slip, an oxidation catalyst or ammonia slip catalyst is incorporated as a final polishing stage. This secondary reactor quantitatively oxidizes residual H_2 slip and fugitive NH_3 into environmentally benign water vapor and atmospheric nitrogen, ensuring compliant near-zero tailpipe emissions across full operating maps [28,60].

6.3. Comprehensive comparison of mitigation strategies

The quantitative impacts of key combustion control and emission-mitigation techniques—including cooled EGR, intake water injection, turbocharging, and turbulent jet ignition—are systematically compiled in Table 5.

Table 5. Comprehensive comparison matrix of mitigation strategies in port hydrogen engines.

Key studies	Mitigation strategy	Primary working mechanism	NO_x reduction capability	Impact on thermal efficiency (BTE)	Impact on power density (BMEP)	Control of backfire and abnormal combustion
Bao et al. [28], Mohamed et al. [16]	Ultra-lean burn (λ = 2.0–3.5)	Excess air dilution lowers peak combustion temperature (Tmax < 1800 K)	Near-zero (< 10–20 ppm, > 95% reduction)	High BTE (approximately 35%–41%) at partial load conditions [11]	Severe penalty (15%–30% loss due to air displacement and dilution)	Suppresses knock and pre-ignition; reduces backfire risk
Krishnan et al. [56], Saravanan et al. [61]	Cooled exhaust gas recirculation (cooled EGR) (12%–28%)	Inert gas (N_2, H_2O) increases charge heat capacity, lowering peak temperature	Very high (57%–74.6% in PFI; up to 84.4% in LDI)	Moderate BTE (approximately 31%–36%); low pumping losses	High (23%–29% higher torque than lean burn at equivalent text NO_x thresholds)	Strongly mitigates backfire and knock by dampening flame propagation speed
Dhyani and Subramanian [44], Zhou et al. [17]	Port water injection (port WI) (WHR 1.0–7.5)	Latent heat of vaporization quenches in-cylinder hot spots and cools intake charge	Exceptional (approximately 97% reduction in NO_x at WHR 7.5)	Improves ITE due to reduced wall heat transfer losses	Maintains high power output; enables higher boost and compression ratios	Absolute/exceptional (eliminates backfire, pre-ignition, and knock)
Lu et al. [11], Marwaha and Subramanian [21]	Safe-zone injection tuning (safe-zone SOI)	Early injection in Zone A (430°–360° ATDC); elevated injection pressure	Indirect NO_x reduction (prevents rich-mixture clusters)	Neutral to slight increase (improves mixture homogeneity and volumetric efficiency)	Minimal impact; dual-injector setup increases peak brake power by 42.3%	Very high backfire control (purges hydrogen from intake port before IVC)
Marwaha and Subramanian [21]	Variable valve timing and spark delay (VVT and spark delay)	LIVO eliminates internal EGR backflow; delaying CA50 lowers peak pressure/ temperature	Very high (rapid NO_x reduction by delaying spark timing ST)	Slight BTE penalty (1%–2.5%, recoverable via turbo charging)	Slight BMEP reduction (2%–5%)	High (LIVO prevents hot exhaust gas backflow into intake; delaying spark eliminates knock)

Continued on next page

Key studies	Mitigation strategy	Primary working mechanism	NO_x reduction capability	Impact on thermal efficiency (BTE)	Impact on power density (BMEP)	Control of backfire and abnormal combustion
Lu et al. [11], Lu et al. [23]	Direct injection transition (DI/LDI/hybrid)	Injects hydrogen directly into the cylinder after intake valve closure (IVC)	Moderate to high (requires EGR or lean burn to suppress thermal NO_x)	Highest BTE (approximately 41%–42.6%; lower pumping and wall heat transfer losses)	Highest (15%–30% power density over PFI; zero air displacement effect)	100% backfire immunity; eliminates pre-ignition in the intake manifold

7. Current challenges and future research needs

7.1. Hardware durability and tribology

The challenges associated with mixture formation and combustion control in hydrogen internal combustion engines stem directly from the unique physicochemical properties of the fuel, which necessitate complex engineering strategies to ensure both performance and operational safety [22,45]. Regarding mixture formation, the volumetric displacement of air by gaseous hydrogen, often termed the air displacement effect, results in hydrogen occupying approximately 30% of the combustion chamber volume at stoichiometric conditions. This phenomenon significantly restricts volumetric efficiency, culminating in a 15%–30% power loss compared to equivalently sized gasoline counterparts in port fuel injection configurations [11,62]. Furthermore, the exceptionally low minimum ignition energy of 0.02 mJ and wide flammability limits make the PFI system highly susceptible to backfire, where the fresh charge is prematurely ignited by hot residuals, glowing hot spots, or abnormal spark plug discharge before the intake valve closes [22]. Compounding these issues, while hydrogen's high mass diffusivity facilitates rapid mixture homogenization, it severely hinders stratified-charge combustion strategies; the fuel tends to disperse uncontrollably toward the cylinder walls and crevices, thereby failing to maintain the localized, rich air-fuel zone around the spark plug that is fundamentally required to stabilize ultra-lean combustion [63].

In terms of combustion control, H2ICES face severe thermodynamic hurdles, primarily driven by rapid flame propagation and high adiabatic flame temperatures, which invariably trigger thermal NO_x formation via the Zeldovich mechanism [11,17,36]. Although operating in hyper-lean regimes (lambda > 2.0) successfully suppresses peak in-cylinder temperatures, thereby mitigating NO_x emissions to near-zero levels, this strategy inherently penalizes power density and induces severe combustion instability [11,36]. Under heavily diluted conditions, the laminar burning velocity drops precipitously, leading to an unacceptable cyclic dispersion quantified by elevated coefficients of variation in the indicated mean effective pressure, severe pressure oscillations, and an increased risk of outright misfire, thus necessitating the implementation of high-energy ignition sources or TJI systems [3,24]. Moreover, the extremely rapid heat release rate renders hydrogen engines exceptionally vulnerable to heavy engine knock and pre-ignition induced by uncontrolled thermal nucleation sites, thereby generating destructive high-amplitude pressure waves that threaten structural components such as pistons and connecting rods while drastically shrinking the safe high-load operating envelope.

Finally, the deployment of hydrogen powertrains is severely restricted by persistent hardware and material limitations, particularly regarding extreme sealing integrity and structural durability [17,30,31]. Due to hydrogen's diminutive molecular size and low viscosity, the fuel readily permeates standard elastomeric materials and escapes through microscopic clearances in injection systems, necessitating advanced sealing technologies and precise manufacturing tolerances [17,31]. Furthermore, hydrogen's lack of natural lubricity accelerates the mechanical wear and frictional losses of moving components within high-pressure fuel pumps and injectors, directly compromising long-term operational reliability. Most critically, hydrogen embrittlement poses a profound metallurgical threat: atomic hydrogen can diffuse into the metallic crystal lattices of engine hardware, inducing localized lattice strain that renders conventional steels and alloys highly susceptible to catastrophic brittle fracture [17]. Consequently, the commercial viability and mechanical integrity of next-generation H2ICEs depend strictly on the integration of specialized, hydrogen-resistant materials, such as austenitic stainless steels or advanced barrier coatings, throughout the entire fuel delivery and combustion architecture.

The optimization of H2ICEs presents profound trade-offs between power density and thermal

NO_x emissions. Although hydrogen is carbon-free, its high adiabatic flame temperature drives thermal NO_x generation via the Zeldovich mechanism at stoichiometric ratios. While adopting ultra-lean burn strategies (lambda > 2.0) successfully quenches peak in-cylinder temperatures below the 1500 ℃ threshold, it inherently slashes power density by 50% or more compared to gasoline baselines. This power deficit is exacerbated in PFI engines by a severe air-displacement effect, in which gaseous hydrogen occupies up to 30% of the cylinder volume, restricting the fresh air mass and causing a 15%–30% power loss.

Hyper-lean operation also severely degrades cyclic combustion stability and increases vulnerability to abnormal combustion. As mixture dilution increases, laminar flame speed drops precipitously, thereby escalating cycle-to-cycle variations and misfire risks. Advanced technologies such as Turbulent Jet Ignition can stabilize these ultra-lean regimes, yet they add mechanical complexity and may exacerbate knocking tendencies. Furthermore, hydrogen's exceptionally broad flammability limits and ultra-low ignition energy make the engine highly susceptible to backfire, pre-ignition, and knock. In PFI systems, residual hot gases readily ignite the incoming charge, causing backfire. Under high loads, hydrogen's rapid heat release triggers violent detonation despite its research octane number exceeding 130. Conventional knock mitigations, such as spark timing delay, provide immediate relief but directly penalize thermal efficiency and torque.

Finally, severe hardware, control, and metallurgical hurdles limit commercial viability. Recovering power density in lean regimes requires massive intake boosting; however, the low enthalpy and reduced temperatures of lean hydrogen exhaust provide insufficient kinetic energy to drive standard turbines, making turbocharger matching a critical bottleneck. At the component level, hydrogen's negligible lubricity and viscosity accelerate frictional wear, rapidly degrading high-pressure injectors and pumps. Moreover, its diminutive molecular size enables persistent permeation through conventional seals. Most critically, atomic hydrogen induces hydrogen embrittlement in highly stressed metallic components, precipitating catastrophic brittle micro-cracking. Consequently, overcoming these intertwined challenges requires a holistic redesign utilizing active thermal diluents—such as cooled EGR or water injection—alongside advanced hydrogen-resistant alloys and precise barrier coatings.

7.2. Modeling and experimental research needs

The continuous advancement of hydrogen internal combustion engines necessitates significant developments in computational simulation methodologies to capture complex thermodynamic and physicochemical phenomena accurately [22]. Primarily, there is a critical imperative to formulate high-fidelity, detailed chemical kinetic mechanisms capable of precisely predicting combustion characteristics—most notably, the laminar burning velocity—under realistic engine boundary conditions characterized by elevated pressures and temperatures. This refinement is essential to rectify the prevailing tendency of current macroscopic models to systematically overestimate LBV in highly diluted lean mixtures. Concurrently, high-resolution 3D CFD frameworks must be deployed to rigorously quantify localized mixture stratifications and isolate instantaneous nucleation sites for NO_x formation [27]. Within this computational domain, LES techniques are indispensable for explicitly resolving CCV and elucidating their subsequent impact on knock propagation—a highly transient, multidimensional phenomenon that standard RANS models inherently fail to adequately resolve [53]. Furthermore, prioritizing the development of robust, high-accuracy predictive models that can reliably forecast backfire probability, knock propensity, and extreme pressure oscillations remains a paramount objective for guiding and optimizing empirical engine calibration. Finally, comprehensive numerical

investigations must seamlessly integrate transient structural modeling of under-expanded supersonic hydrogen jets with precise boundary-layer representations of near-wall heat-transfer mechanisms to systematically mitigate critical thermal losses and improve overall predictive fidelity.

The empirical validation of hydrogen internal combustion engine advancements demands extensive experimental investigations across several critical domains. Primarily, the fundamental characteristics of abnormal combustion necessitate deeper exploration, specifically regarding the precise prediction, propagation velocity, and quenching mechanisms of backfire, coupled with the urgent establishment of standardized, non-controversial knock-resistance metrics specifically tailored for hydrogen, transcending conventional RON/MON methodologies [3,22]. To rigorously validate high-fidelity 3D CFD models, advanced optical diagnostics—such as high-speed Schlieren imaging, PLIF, and Raman spectroscopy—remain absolutely vital for capturing spatially and temporally resolved data concerning mixture preparation, early flame kernel development, and flame-wall interactions [45,64]. Furthermore, hardware optimization must be aggressively pursued, including the industrial development of durable, high-flow hydrogen injectors with absolute sealing integrity, as well as the geometric refinement of nozzle configurations, piston bowl geometries, and liquid-cooled spark plugs. Scaling up these experimental paradigms to heavy-duty, medium-speed, large engines is also imperative for accurately mapping operational boundaries and classifying abnormal combustion phenomena that are demanding for these engines [31]. Finally, comprehensive experimental sweeps across the entire engine operating map are required to effectively manage the complex trade-offs between power output and thermal NO_x emissions through hyper-lean burn, exhaust gas recirculation, and water injection strategies, while concurrently investigating the critical physicochemical impacts of lubricating oils and their respective additives on pre-ignition tendencies [10,32,45].

7.3. Emerging technologies and future perspectives

The future of hydrogen internal combustion engines is marked by a shift toward advanced combustion concepts, novel engine architectures, and the integration of digital optimization tools to overcome existing physical limitations. Moving beyond traditional methods, the industry is heavily investing in next-generation ignition technologies—such as laser-induced, plasma-assisted, and advanced corona ignition systems—to ensure reliable combustion in ultra-lean regimes where conventional sparks fail. Furthermore, turbulent jet ignition pre-chamber systems and plume ignition concepts are being actively developed to accelerate burn rates, improve stability, and mitigate knock [32].

In addition to pure hydrogen operation, future perspectives emphasize the strategic synergy with alternative, carbon-neutral energy carriers. A notable approach involves the ammonia-hydrogen synergy, in which hydrogen acts as a combustion promoter to overcome ammonia' inertness, even paving the way for onboard ammonia decomposition [29]. Another groundbreaking concept is the oxy-hydrogen combustion cycle, which burns hydrogen in pure oxygen instead of air. Combined with direct water injection for temperature control, this pressurized system produces only steam as a byproduct, achieving theoretical thermal efficiencies exceeding 70% [65].

To compensate for hydrogen's low volumetric power density, manufacturers are designing innovative engine architectures that maximize output within compact footprints. Free-piston linear engines eliminate the traditional crank linkage mechanism, enabling variable compression ratios and high power density, making them ideal as lightweight onboard range extenders or generators [1,35]. Similarly, Wankel rotary engines are receiving renewed attention because their rotary architecture inherently delivers the power density of a two-stroke cycle within a four-stroke framework, which perfectly complements hydrogen's low density when optimized with dedicated direct injection [1].

The immense complexity of precisely controlling highly dynamic H2ICE operating parameters—such as injection timing, pressure, exhaust gas recirculation, and spark timing—has driven the integration of digital optimization tools. Artificial intelligence and machine learning algorithms are increasingly deployed to optimize engine performance in real time [17]. These advanced digital systems are crucial for dynamically predicting and detecting abnormal combustion phenomena, such as knock or backfire, before they compromise engine integrity.

On a global scale, industry leaders are aggressively transitioning these technologies from research labs toward mass production and large-scale decarbonization. Heavyweight manufacturers are actively tailoring hydrogen engines for heavy-duty transport and high-performance racing applications [17]. Moreover, pairing H2ICES with electric motors in hybrid powertrains offers functional synergies that achieve near-zero nitrogen oxide emissions and extended driving ranges [1]. Ultimately, the long-term viability of hydrogen combustion relies heavily on infrastructure growth, with projected drops in green hydrogen production costs below $2 USD per kilogram by 2050, positioning hydrogen combustion as a highly competitive alternative to fossil fuels.

8. Conclusions

This review systematically examined mixture preparation, combustion characteristics, abnormal combustion, and emissions in PFI hydrogen spark-ignition engines by synthesizing findings from multidimensional CFD simulations, one-dimensional thermodynamic models, and experimental studies. PFI offers a technically simple and cost-effective pathway for hydrogen engine applications because of its low injection-pressure requirements (0.2–1.0 MPa) and favorable fuel-air premixing; however, hydrogen-induced air displacement can reduce power density by approximately 15%–30%. Appropriate injection phasing, particularly at approximately 20%–30% intake-valve lift, is critical to improve mixture formation while limiting fuel backflow and hydrogen accumulation in the intake system. Hydrogen's high burning velocity and knock resistance enable rapid combustion, high compression ratios, and potentially high thermal efficiency, but its low minimum ignition energy, wide flammability range, and small quenching distance substantially increase susceptibility to backfire, pre-ignition, knock, and super-knock. Moreover, although direct fuel-derived CO_2 emissions are eliminated, thermal NO_x remains the principal regulated pollutant, particularly under stoichiometric and high-load conditions, requiring coordinated application of ultra-lean combustion, cooled EGR, and exhaust aftertreatment.

Further advancement of PFI H2ICE technology requires integrated optimization of mixture formation, combustion phasing, thermal management, boosting, aftertreatment, and engine control, together with improved solutions for tribological wear, hydrogen permeation, and material embrittlement. High-fidelity LES combined with advanced optical diagnostics will be important for resolving transient mixture distributions, flame propagation, cycle-to-cycle variability, and abnormal combustion, while intelligent closed-loop control, advanced ignition systems, and optimized lean-burn boosting offer promising routes toward extending the stable operating range. Overall, PFI H2ICE offers a practical pathway to use existing spark-ignition engine architectures with hydrogen, but broader implementation will depend on achieving a robust balance among power density, thermal efficiency, NO_x control, combustion stability, and long-term durability.

Use of AI tools declaration

The authors used ChatGPT (OpenAI), and Google Gemini solely to improve the language and readability of the manuscript. The authors take full responsibility for the scientific content, data analysis, interpretation, and conclusions presented in this work.

Conflict of interest

The authors declare no conflicts of interest.

Author contributions

Nguyen Duy Vinh conceived the study, supervised the research, and reviewed the manuscript. Hoang Dinh Long contributed to the study design, provided scientific supervision, and critically revised the manuscript. Pham Van Trong conducted the research, performed the data analysis, prepared the figures, and drafted the manuscript. All authors reviewed and approved the final version of the manuscript.

References

1. Sun Z, Hong J, Zhang T, et al. (2023) Hydrogen engine operation strategies: Recent progress, industrialization challenges, and perspectives. *Int J Hydrogen Energy* 48: 366–392. https://doi.org/10.1016/j.ijhydene.2022.09.256
2. Gao N, Geng Z, Zhao W, et al. (2025) Review on the combustion and emission characteristics of hydrogen engine. *Int J Hydrogen Energy* 143: 121–146. https://doi.org/10.1016/j.ijhydene.2025.05.321
3. Stępień Z (2021) A comprehensive overview of hydrogen-fueled internal combustion engines: Achievements and future challenges. *Energies* 14: 6504. https://doi.org/10.3390/en14206504
4. Musy F, Ortiz R, Ortiz I, et al. (2024) Hydrogen-fuelled internal combustion engines: Direct injection versus port-fuel injection. *Int J Hydrogen Energy* 137: 925–938. https://doi.org/10.1016/j.ijhydene.2024.07.136
5. Piano A, Quattrone G, Millo F, et al. (2024) Development and validation of a predictive combustion model for hydrogen-fuelled internal combustion engines. *Int J Hydrogen Energy* 89: 1310–1320. https://doi.org/10.1016/j.ijhydene.2024.09.407
6. Lei H, Zhang Y, Khandelwal B (2025) Numerical investigation of geometric design effect on micromix hydrogen combustion. *Fuel* 401: 135657. https://doi.org/10.1016/j.fuel.2025.135657
7. Habib MA, Abdulrahman GAQ, Alquaity ABS, et al. (2024) Hydrogen combustion, production, and applications: A review. *Alexandria Eng J* 100: 182–207. https://doi.org/10.1016/j.aej.2024.05.030
8. Chen Y, Lou D, Zhang Y, et al. (2024) An investigation on the H_2O, unburned H_2 and NO emission characteristics from a direct injection hydrogen engine. *Int J Hydrogen Energy* 81: 1181–1191. https://doi.org/10.1016/j.ijhydene.2024.07.368
9. Rueda-Vázquez JM, Serrano J, Jiménez-Espadafor FJ, et al. (2024) Experimental analysis of the effect of hydrogen as the main fuel on the performance and emissions of a modified compression ignition engine with water injection and compression ratio reduction. *Appl Therm Eng* 238: 121933. https://doi.org/10.1016/j.applthermaleng.2023.121933
10. Gao J, Wang X, Song P, et al. (2022) Review of the backfire occurrences and control strategies for port hydrogen injection internal combustion engines. *Fuel* 307: 121553. https://doi.org/10.1016/j.fuel.2021.121553
11. Lu Y, Que J, Xia Y, et al. (2024) A comparative study of the effects of EGR on combustion and emission characteristics of port fuel injection and late direct injection in hydrogen internal combustion engine. *Appl Energy* 375: 123830. https://doi.org/10.1016/j.apenergy.2024.123830

12. Khalid AH, Muhamad Said MF, Veza I, et al. (2024) Hydrogen port fuel injection: Review of fuel injection control strategies to mitigate backfire in internal combustion engine fuelled with hydrogen. *Int J Hydrogen Energy* 66: 571–581. https://doi.org/10.1016/j.ijhydene.2024.04.087
13. Yun H, Bu Z, Yang Z, et al. (2023) Optimization of fuel injection timing and ignition timing of hydrogen fueled SI engine based on DOE-MPGA. *Int J Hydrogen Energy* 48: 9462–9473. https://doi.org/10.1016/j.ijhydene.2022.12.068
14. Liang Z, Xie F, Lai K, et al. (2024) Study of single and split injection strategies on combustion and emissions of hydrogen DISI engine. *Int J Hydrogen Energy* 49: 1087–1099. https://doi.org/10.1016/j.ijhydene.2023.10.060
15. Piano A, Pucillo F, Millo F, et al. (2025) Experimental investigation on the optimal injection and combustion phasing for a direct injection hydrogen-fuelled internal combustion engine for heavy-duty applications. *Int J Hydrogen Energy* 100: 398–406. https://doi.org/10.1016/j.ijhydene.2024.12.194
16. Mohamed M, Longo K, Zhao H, et al. (2024) Hydrogen engine insights: A comprehensive experimental examination of port fuel injection and direct injection. *SAE Technical Papers*. https://doi.org/10.4271/2024-01-2611
17. Zhou F, Wu C, Fu J, et al. (2025) Abnormal combustion and NOx emissions control strategies of hydrogen internal combustion engine. *Renew Sustain Energy Rev* 219: 115847. https://doi.org/10.1016/j.rser.2025.115847
18. Do TT, Tang Y, Dang ND, et al. (2025) Research on the implementation of hydrogen in small spark ignition engines. *Vietnam J Agric Sci* 8: 2385–2394. https://doi.org/10.31817/vjas.2025.8.1.04
19. Kumar V, Gupta D, Kumar N (2015) Hydrogen use in internal combustion engine: A review. *Int J Adv Cult Technol* 3: 87–99. https://doi.org/10.17703/IJACT.2015.3.2.87
20. Gomes Antunes JM, Mikalsen R, Roskilly AP (2009) An experimental study of a direct injection compression ignition hydrogen engine. *Int J Hydrogen Energy* 34: 6516–6522. https://doi.org/10.1016/j.ijhydene.2009.05.142
21. Marwaha A, Subramanian KA (2024) Experimental investigation on backfire occurrence, duration and termination in a hydrogen-fueled automotive spark ignition engine. *Process Saf Environ Prot* 189: 322–342. https://doi.org/10.1016/j.psep.2024.06.091
22. Kinkhabwala B, Krishna K, Reppert F, et al. (2025) An experimental and computational analysis of backfire initiation and propagation in a single-cylinder hydrogen port-fuel-injection engine. *Automot Engine Technol* 10: 16. https://doi.org/10.1007/s41104-025-00163-9
23. Lu Y, Que J, Liu M, et al. (2024) Study on backfire characteristics of port fuel injection single-cylinder hydrogen internal combustion engine. *Appl Energy* 364: 123110. https://doi.org/10.1016/j.apenergy.2024.123110
24. Rao X, Lou D, Zhang Y, et al. (2025) Experimental investigation and multi-objective optimization of combustion characteristics and performance in a port-fuel-injected hydrogen engine. *Int J Hydrogen Energy* 192: 152370. https://doi.org/10.1016/j.ijhydene.2025.152370
25. Bayramoğlu K, Yılmaz S (2021) Emission and performance estimation in hydrogen injection strategies on diesel engines. *Int J Hydrogen Energy* 46: 29732–29744. https://doi.org/10.1016/j.ijhydene.2020.08.135
26. Wang Y, Verhelst S (2024) Comparative analysis and optimisation of hydrogen combustion mechanism for laminar burning velocity calculation in combustion engine modelling. *Int J Hydrogen Energy* 56: 880–893. https://doi.org/10.1016/j.ijhydene.2023.12.214

27. Zhao FC, Sun BG, Yuan S, et al. (2024) Experimental and modeling investigations to improve the performance of the near-zero NOx emissions direct-injection hydrogen engine by injection optimization. *Int J Hydrogen Energy* 49: 713–724. https://doi.org/10.1016/j.ijhydene.2023.09.039
28. Bao LZ, Sun BG, Luo QH, et al. (2022) Development of a turbocharged direct-injection hydrogen engine to achieve clean, efficient, and high-power performance. *Fuel* 324: 124713. https://doi.org/10.1016/j.fuel.2022.124713
29. Qi Y, Liu W, Liu S, et al. (2023) A review on ammonia-hydrogen fueled internal combustion engines. *ETransportation* 18: 100288. https://doi.org/10.1016/j.etran.2023.100288
30. Wittek K, Cogo V, Prante G (2023) Development of a pneumatic actuated low-pressure direct injection gas injector for hydrogen-fueled internal combustion engines. *Int J Hydrogen Energy* 48: 10215–10234. https://doi.org/10.1016/j.ijhydene.2022.12.023
31. Hu Z, Yuan S, Wei H, et al. (2024) High-pressure injection or low-pressure injection for a direct injection hydrogen engine? *Int J Hydrogen Energy* 59: 383–389. https://doi.org/10.1016/j.ijhydene.2024.02.018
32. Pandey JK, Kumar GN (2022) Effect of variable compression ratio and equivalence ratio on performance, combustion and emission of hydrogen port injection SI engine. *Energy* 239: 122468. https://doi.org/10.1016/j.energy.2021.122468
33. Molina S, Novella R, Gomez-Soriano J, et al. (2024) Impact of medium-pressure direct injection in a spark-ignition engine fueled by hydrogen. *Fuel* 360: 130618. https://doi.org/10.1016/j.fuel.2023.130618
34. Zhang SW, Sun BG, Lin SL, et al. (2024) Energy and exergy analysis for a turbocharged direct-injection hydrogen engine to achieve efficient and high-economy performances. *Int J Hydrogen Energy* 54: 601–612. https://doi.org/10.1016/j.ijhydene.2023.04.038
35. Qin Z, Zhang H, Liu F, et al. (2024) A coupled study of injection strategy on gas motion and heat transfer in a diesel ignition linear hydrogen engine. *Int J Hydrogen Energy* 82: 502–512. https://doi.org/10.1016/j.ijhydene.2024.07.444
36. Lu Y, Wang Q, Qin L, et al. (2025) Comparison between homogeneous combustion and stratified combustion caused by direct injection timing adjustment in lean-burn hydrogen internal combustion engine. *Int J Hydrogen Energy* 103: 1–11. https://doi.org/10.1016/j.ijhydene.2024.12.469
37. Houidi MB, Moreno-Cabezas K, Zaihi A, et al. (2024) Investigating hydrogen direct injection technology: A comparative analysis of nozzle geometries for enhanced mixing in internal combustion engines. *Proc Combust Inst* 40: 105631. https://doi.org/10.1016/j.proci.2024.105631
38. Babayev R, Andersson A, Serra Dalmau A, et al. (2022) Computational comparison of the conventional diesel and hydrogen direct-injection compression-ignition combustion engines. *Fuel* 307: 121909. https://doi.org/10.1016/j.fuel.2021.121909
39. Chen Y, Raine R (2014) Engine knock in an SI engine with hydrogen supplementation under stoichiometric and lean conditions. *SAE Int J Engines* 7: 595–605. https://doi.org/10.4271/2014-01-1220
40. Zhang H, Li G, Long Y, et al. (2023) Numerical study on combustion and emission characteristics of a spark-ignition ammonia engine added with hydrogen-rich gas from exhaust-fuel reforming. *Fuel* 332: 125939. https://doi.org/10.1016/j.fuel.2022.125939
41. Ye Y, Gao W, Li Y, et al. (2020) Numerical study of the effect of injection timing on the knock combustion in a direct-injection hydrogen engine. *Int J Hydrogen Energy* 45: 27904–27919. https://doi.org/10.1016/j.ijhydene.2020.07.117
42. Duan YH, Sun BG, Li Q, et al. (2023) Combustion characteristics of a turbocharged direct-injection hydrogen engine. *Energy Convers Manag* 291: 117267. https://doi.org/10.1016/j.enconman.2023.117267

43. Chen W, Lu C, Zuo Q, et al. (2024) Combustion characteristics analysis and performance evaluation of a hydrogen engine under direct injection plus lean burn mode. *J Clean Prod* 470: 143323. https://doi.org/10.1016/j.jclepro.2024.143323
44. Dhyani V, Subramanian KA (2021) Development of online control system for elimination of backfire in a hydrogen fuelled spark ignition engine. *Int J Hydrogen Energy* 46: 14757–14763. https://doi.org/10.1016/j.ijhydene.2020.08.148
45. Deist SO, Zepf A, Winkler D, et al. (2025) Endoscopic visualization of backfire behavior in a medium speed maritime hydrogen engine. *Int J Hydrogen Energy* 169: 150938. https://doi.org/10.1016/j.ijhydene.2025.150938
46. Faizal M, Chuah LS, Lee C, et al. (2019) Review of hydrogen fuel for internal combustion engines. *J Mech Eng Res Dev* 42: 36–46. https://doi.org/10.26480/jmerd.03.2019.35.46
47. Menaa A, Lounici MS, Amrouche F, et al. (2019) CFD analysis of hydrogen injection pressure and valve profile law effects on backfire and pre-ignition phenomena in hydrogen-diesel dual fuel engine. *Int J Hydrogen Energy* 44: 9408–9422. https://doi.org/10.1016/j.ijhydene.2019.02.123
48. Algayyim SJM, Saleh K, Wandel AP, et al. (2024) Influence of natural gas and hydrogen properties on internal combustion engine performance, combustion, and emissions: A review. *Fuel* 362: 130844. https://doi.org/10.1016/j.fuel.2023.130844
49. Liang Z, Xie F, Guo Z, et al. (2024) Optimization and prediction of a novel preignition in hydrogen direct injection engines through experimentation and the random forest algorithms. *Energy Convers Manag* 313: 118602. https://doi.org/10.1016/j.enconman.2024.118602
50. Guo S, Liu J, Zhao C, et al. (2024) Research on pre-ignition in hydrogen internal combustion engines based on characteristic parameters of hot spot. *Int J Hydrogen Energy* 65: 548–554. https://doi.org/10.1016/j.ijhydene.2024.03.375
51. Liang Y, Xing K, Huang H, et al. (2025) Investigation of knock combustion mechanism and injection angle optimization in a heavy-duty direct-injection hydrogen engine. *Energy* 335: 138041. https://doi.org/10.1016/j.energy.2025.138041
52. Lou D, Rao X, Zhang Y, et al. (2024) Investigation of impacts of hydrogen injection and spark strategy on knock in hydrogen engine. *Int J Hydrogen Energy* 82: 1252–1262. https://doi.org/10.1016/j.ijhydene.2024.08.052
53. Manzoor MU, Dou X, Yosri MR, et al. (2024) Capturing different modes of hydrogen combustion in a spark-ignition engine using numerical simulations. *Fuel* 375: 132343. https://doi.org/10.1016/j.fuel.2024.132343
54. Sementa P, Tornatore C, Catapano F, et al. (2025) Impact of injection parameters on hydrogen combustion: Flame propagation and stability in ultra-lean mixtures. *Int J Hydrogen Energy* 143: 615–626. https://doi.org/10.1016/j.ijhydene.2025.04.091
55. Wei H, Hu Z, Ma J, et al. (2023) Experimental study of thermal efficiency and NOx emission of turbocharged direct injection hydrogen engine based on a high injection pressure. *Int J Hydrogen Energy* 48: 12905–12916. https://doi.org/10.1016/j.ijhydene.2022.12.031
56. Krishnan Unni J, Bhatia D, Dutta V, et al. (2017) Development of hydrogen fuelled low NOx engine with exhaust gas recirculation and exhaust after treatment. *SAE Int J Engines* 10: 46–54. https://doi.org/10.4271/2017-26-0074
57. Bao LZ, Sun BG, Luo QH (2022) Optimal control strategy of the turbocharged direct-injection hydrogen engine to achieve near-zero emissions with large power and high brake thermal efficiency. *Fuel* 325: 124913. https://doi.org/10.1016/j.fuel.2022.124913
58. Bibiloni-Ipata S, Martinez-Boggio S, Merola S, et al. (2026) Simulation analysis of a spark-ignition engine fueled with gasoline and hydrogen. *Fire* 9: 4. https://doi.org/10.3390/fire9010004
59. Brancaleoni PP, Corti E, Ravaglioli V, et al. (2024) Innovative torque-based control strategy for hydrogen internal combustion engine. *Int J Hydrogen Energy* 73: 203–220. https://doi.org/10.1016/j.ijhydene.2024.05.481

60. Zuo Q, Yang D, Shen Z, et al. (2025) Effect of premixed ratio on combustion and emission characteristics in a spark ignition engine with hydrogen-ammonia direct injection. *Fuel* 393: 135051. https://doi.org/10.1016/j.fuel.2025.135051
61. Saravanan N, Nagarajan G (2010) An experimental investigation on hydrogen fuel injection in intake port and manifold with different EGR rates. *Int J Energy Environ* 1: 221–248. https://api.semanticscholar.org/CorpusID:231968026
62. Bao LZ, Sun BG, Luo QH, et al. (2020) Experimental study of the polytropic index of the compression stroke for a direct injection hydrogen engine. *Int J Hydrogen Energy* 45: 28196–28203. https://doi.org/10.1016/j.ijhydene.2020.03.006
63. Yang Z, Zhang F, Wang L, et al. (2018) Effects of injection mode on the mixture formation and combustion performance of the hydrogen internal combustion engine. *Energy* 147: 715–728. https://doi.org/10.1016/j.energy.2018.01.068
64. Welch C, Erhard J, Shi H, et al. (2024) An experimental investigation of lean hydrogen flame instabilities in spark-ignition engines. *Proc Combust Inst* 40: 105391. https://doi.org/10.1016/j.proci.2024.105391
65. Boretti A (2024) A high-efficiency internal combustion engine using oxygen and hydrogen. *Int J Hydrogen Energy* 50: 847–856. https://doi.org/10.1016/j.ijhydene.2023.08.363



AIMS Press

© 2026 the Author(s), licensee AIMS Press. This is an open access article distributed under the terms of the Creative Commons Attribution License (https://creativecommons.org/licenses/by/4.0)